THESIS FOR THE DEGREE OF LICENTIATE OF ENGINEERING

Strongly Correlated Inhomgeneous High-Temperature Superconductors

AMBJÖRN JOKI

Department of Microtechnology and Nanoscience (MC2)
CHALMERS UNIVERSITY OF TECHNOLOGY

Göteborg, Sweden 2025

Strongly Correlated Inhomgeneous High-Temperature Superconductors

AMBJÖRN JOKI

Thesis for the degree of Licentiate of Engineering
ISSN 1652-0769
Technical Report MC2-475

Chalmers University of Technology
Department of Microtechnology and Nanoscience (MC2)
Applied Quantum Physics Laboratory
SE-412 96 Göteborg, Sweden
Telephone: +46 (0)31-772 1000

Cover
Square lattice with basic interactions of the t–J model high included, see Figure 2.1 for further details.

Printed by Chalmers Reproservice
Göteborg, Sweden 2025

Strongly Correlated Inhomgeneous High-Temperature Superconductors
Thesis for the degree of Licentiate of Engineering

AMBJÖRN JOKI

Department of Microtechnology and Nanoscience (MC2)
Applied Quantum Physics Laboratory
Chalmers University of Technology

Abstract

Since its discovery, superconductivity has received significant attention, with renewed interest following the discovery of high-temperature superconductors (HTSCs) such as cuprates. The t–J model, combined with the Gutzwiller approximation, has been used to study HTSCs. While much research has focused on homogeneous systems, less attention has been given inhomogeneous ones – especially the possible coexistence of superconductivity and antiferromagnetism in them. The coexistence could be of interest for applications within superconducting spintronics.

The focus of the present thesis is [110] edges of HTSCs. It is shown that these edges attract quasiparticles, increasing the local occupation and thereby strengthening local correlation, which in turn reduces the weight of the zero-energy Andreev bound states typically present at [110] edges. Furthermore, the s-wave order parameter, predicted in some models to form at the edge, is here seen to vanish or be suppressed. Finally, it is demonstrated that the charging of the edges enables antiferromagnetic order to emerge at the edges at higher average dopings than in homogeneous systems.

Keywords: inhomogenous superconductors, cuprates, strong electron-electron interactions, Gutzwiller approximation, mean-field theory, [110] edges, t–J model

Acknowledgements

First, I would like to thank my supervisor Tomas Löfwander for all his help with the paper this thesis is based on, and for his valuable feedback on the thesis itself. I also wish to thank my examiner, Mikael Fogelström, for his help.

I would also like to thank my former co-supervisor and officemate, Kevin, for all his support during my early PhD years. And not least, I want to thank everyone who has patiently listened to my endless advice on gardening.

List of publications

This thesis presents a summary and an extension to the following appended paper:

[I] A. Joki, M. Fogelström, and T. Löfwander, "Strengthened correlations near [110] edges of d-wave superconductors in the tJ model with the Gutzwiller approximation", arXiv preprint arXiv:2507.08398 (2025).

The paper is always referred to as paper I.

List of figures

1.1 Order parameters in reciprocal space. (a) The uniform s-wave order parameter independent of momentum direction (b) the momentum dependent d-wave order parameter, zero at the nodes. 2

1.2 Structure of YBCO with copper in green, oxygen in grey, barium in orange, and yttrium in purple. From [11] with relabelled axes. . . 2

1.3 Generic examples of the gap in the density states of superconductor with (a) s-wave and (b) d-wave symmetry. The DOS is on the y-axis normalised by the DOS in a normal metal N_F and the energy, expressed in the units of the Boltzmann factor times transition temperature, is on the x-axis. 3

2.1 Square lattice where blue arrows at green sites indicate the spins of electrons, t is the hopping amplitude and J the exchange coupling. The black lines indicate links and there are fewer electrons than sites, indicating a hole-doped system. The lattice axes x and y are marked as well as the lattice constant d. 8

2.2 Possible symmetries of the superconductivity on a square lattice in real space. In (a) the s-wave, same order parameter Δ in all directions, is shown, in (b) the d-wave where there is a sign difference between links in the x- and y-direction, in (c) the p_x-wave and in (d) the p_y-wave, the sign of the order parameter is opposite of that on the previous link in the two latter cases. 9

4.1 A homogeneous lattice with the magnetic unit cell marked with red lines. The cell contains one A-site in the center and one B-site. The latter in the form of four quarters of neighbouring B-sites, placed in the corners of the unit cell. The lattice constant d, and the x- and y-axes are marked as well as the symmetry axes in reciprocal space x' and y'. 20

4.2 First row, mean-fields for $J = 0.25$ in (a) and multiplied by the appropriate Gutzwiller factor in (b), second row, mean-fields for $J = 1$ in (c) and multiplied by the appropriate Gutzwiller factor in (d), according to legends. The entire considered doping region is plotted, as specified on the x-axes. 26

4.3 Focus on the region with coexistence of superconductivity and antiferromagnetism. First row, mean-fields for $J = 0.25$ in (a) and multiplied by the appropriate Gutzwiller factor in (b), second row, mean-fields for $J = 1$ in (c) and multiplied by the appropriate Gutzwiller factor in (d), according to legends. Dopings are specified at the x-axes. 27

4.4 Lagrange multipliers for J=0.25 in (a)-(b) and J=1 in (c)-(d). The left column shows the entire studied doping interval while the right focuses on the region with coexsistence. 28

4.5 DOS of up spins at sites A at hole doping $\delta = 0.05$ and with $J = 0.25$, at the y-axis, see Equation (4.22), and energy on the x-axis. The system is in the non-antiferromagnetic region and therefore spin down will look the same. 29

4.6 Results for $\delta = 0.005$ in (a) DOS of spin up using J=0.25 (b) DOS of spin up using J=1 and (c) DOS of spin down using J=1. In all, the x-axis gives energy and the DOS, see Equation (4.22), is on the y-axis. In (a) the system is in the non-antiferromagnetic region and therefore spin down will look the same. In (b) and (c) the system is in the region with coexistence so the DOS of both spin up and down are plotted since they are different. 30

5.1 (a) The studied slab with sites, as grey disks, arranged into a square lattice with lattice constant d. The edges are cut in the [110]-direction. Red lines mark the unit cell and translational invariance along the edge tangent is assumed. The x- and y-axes are the crystal axes, corresponding to the x- and y-axes in Figure 1.2. Between sites the lines represents links which can be in either x- or y-direction. In (b) enlarged view of the area surrounded by dotted blue lines in (a), including the right [110] edge. The symmetry axes x' and y' of the unit cell are marked. The axes are chosen so that y' is aligned with the edge tangent and x' with the edge normal. The sites in the unit cell are labelled $a = 1, 2, 3$, etc. after their distance to the right edge measured along x'. Note that it is important to differentiate between the pairing amplitudes $\Delta^x_{a,a+1}$ and $\Delta^y_{a,a+1}$ if both d-wave and extended s-wave symmetries should be considered. There is one link in the y-direction and one in the x-direction between each pair of sites a and $a + 1$. Same Figure as Figure 1 in Paper I. 33

5.2 (a) Spatially dependent electron densities n_a, (b) hopping amplitude $\chi_{a,a+1}$, (c) combination of pairing amplitudes corresponding to d-wave character $(\Delta^x_{a,a+1} - \Delta^y_{a,a+1})/2$, (d) combination of pairing amplitudes corresponding to s-wave character $(\Delta^x_{a,a+1} + \Delta^y_{a,a+1})/2$ multiplied by the negative imaginary unit $-i$, (c) combination of superconducting order parameters corresponding to d-wave character $(\Delta^{\mathrm{SC,x}}_{a,a+1} - \Delta^{\mathrm{SC,y}}_{a,a+1})/2$ and (f) combination of superconducting order parameters corresponding to s-wave character $(\Delta^{\mathrm{SC,x}}_{a,a+1} + \Delta^{\mathrm{SC,y}}_{a,a+1})/2$ once more multiplied by $-i$. All quantities are for $\delta = 0.80$ given in the legend. The slab width is $N_x = 100$, but only the first $a \in [1, 30]$ sites/links are shown. 39

5.3 Local density of states $\Gamma\mathcal{N}_a(\omega)$ for $N_x = 100$, $\delta = 0.8$ and $J = 0.3$. In (a) the full spectrum as function of coordinate a is shown using $\Gamma = 0.015$. (b) Focus on the low-energy part of the spectrum, where the zero-energy Andreev bound states are clearly seen as well as the split of them due to the s-wave component, generated with a smaller $\Gamma = 0.001$. 40

5.4 Results for average hole doping $\delta = 0.03$ using J=1. In (a) the occupation is plotted and in (b) the magnetisation. The singlet superconductivity, $\Delta^x_{a,a+1,\uparrow} - \Delta^x_{a,a+1,\downarrow}$, in (c) and the triplet, $\Delta^x_{a,a+1,\uparrow} + \Delta^x_{a,a+1,\downarrow}$, in (d). In (e) and (f) the superconducting order parameter is shown, singlet, $\Delta^{\mathrm{SC},x}_{a,a+1,\uparrow} - \Delta^{\mathrm{SC},x}_{a,a+1,\uparrow}$ and triplet, $\Delta^{\mathrm{SC},x}_{a,a+1,\uparrow} + \Delta^{\mathrm{SC},x}_{a,a+1,\uparrow}$, respectively. In (g) the hopping mean-field is plotted. In (a)-(g) the legend in (a) indicates the occupations. In (h) the spin dependent Gutzwiller factors for hopping and superconductivity are plotted as stated by the legend. All plots are having site number on the x-axis. 42

5.5 The full DOS in (a) as a function of coordinate a generated using $\Gamma = 0.015$, $J = 1$ and $\delta = 0.03$. (b) Focuses on the region of the energy gap of the spectrum, where the zero-energy Andreev bound states and their split are seen, generated using $\Gamma = 0.001$. 43

5.6 Cuts of the LDOS for sites and spins indicated by the legends. The left colon shows a wider energy spectrum while the right is focused on the gap region. Note that the sites in (d) and (e) are different to (i) and (j). All generated at $\delta = 0.03$ and using $J = 1$. 44

Contents

Abstract iii

Acknowledgements v

List of publications vii

List of figures ix

Contents xiii

1 Introduction 1
- 1.1 Superconductivity . . . 1
  - 1.1.1 Cuprates . . . 2
- 1.2 Inhomogeneous Cuprates With Strong Electron-Electron Interactions 3
- 1.3 Outline of Thesis . . . 4

2 Modelling Superconductors 5
- 2.1 BCS Theory . . . 5
- 2.2 t–J model . . . 7
  - 2.2.1 Symmetries on a Square Lattice . . . 9

3 Gutzwiller Approaches 11
- 3.1 Gutzwiller Factors . . . 11
  - 3.1.1 Fugacity Factors . . . 12
  - 3.1.2 Gutzwiller Factors for Pair of Operators . . . 13
  - 3.1.3 Gutzwiller Factor for Four-Operator Terms . . . 14
- 3.2 Mean-Field Guztwiller Approaches . . . 16

4 Homogenous Case 19
- 4.1 Evaluation of Mean-Field Hamiltonian . . . 19
- 4.2 Self-Consistent Equations and Equations for Lagrange Multipliers 23
- 4.3 Density of States . . . 23
- 4.4 Results . . . 24
  - 4.4.1 Phase Diagrams . . . 25
  - 4.4.2 Density of States . . . 25

5 Inhomogenous Case 31
- 5.1 Evaluation of Mean-Field Hamiltonian . . . 32

5.2 Self-Consistent Equations and Equations for Lagrange Multipliers 35
5.3 Superconductivity Without Antiferromagnetism 37
5.3.1 Summary of Paper I - $J = 0.25$ 37
5.3.2 Higher Exchange Coupling - $J = 0.33$ 38
5.4 Coexistence of Antiferromagnetism and d-Wave Superconductivity - $J = 1$ 38
5.4.1 Mean-Fields 41
5.4.2 Density of States 42

6 Conclusion and Outstanding Questions **45**

References **47**

Appended papers **51**

Paper I **53**

1 Introduction

Essential concepts of the present thesis are high-temperature superconductors (HTSCs), strong electron-electron interactions, and inhomogeneous systems. The introduction is therefore aimed at introducing the, for the thesis, most crucial aspects of these concepts. The first section presents some basics of superconductivity, and some short facts about the HTSC cuprates. In the following section, previous studies of inhomogeneous superconductors (SCs) with strong electron-electron interactions using the $t - J$ model are mentioned. The introduction is concluded by an outline of the thesis.

1.1 Superconductivity

When superconductors (SCs) are cooled below their transition temperature T_c they enter the superconducting phase [1]. The phase is characterised by zero resistivity as a result of an attractive interaction between electrons [2]. The interaction makes the electrons pair [3]. Pairing reduces the combined energy of the electrons and makes pairs less susceptible to scattering. The latter, since breaking a pair is related to an energy cost of two times the superconducting order parameter 2Δ.

Mercury was the first material reported to be superconducting in 1911 by Kamerlingh Onnes [4]. The metal has a low transition temperature of about $T_c = 4.15$ K dependent on phase [5] and the attractive interaction is believed to be mediated by phonons. Thus, mercury has an isotropic order parameter [2] which has s-wave symmetry, see Figure 1.1(a) for a representation of the symmetry in reciprocal space. The labelling agrees with that of atomic orbitals. Mercury and other conventional SCs are well described by the original Bardeen-Cooper-Schrieffer (BCS) theory, see Section 2.1.

Later superconductivity in heavy-fermion systems [6, 7], organic SCs [8] and high-temperature superconductors (HTSCs) was found, they exhibit strong electron-electron interactions, these are called strongly correlated SCs [2]. The mechanism behind the superconductivity in these materials is not established. Some of these are having an order parameter with d-wave symmetry, see Figure 1.1(b). A d-wave order parameter is zero for some directions, the nodes. The lower symmetry of the order parameter, means these materials break space-symmetry entering the superconducting phase. These superconductors are referred to as unconventional.

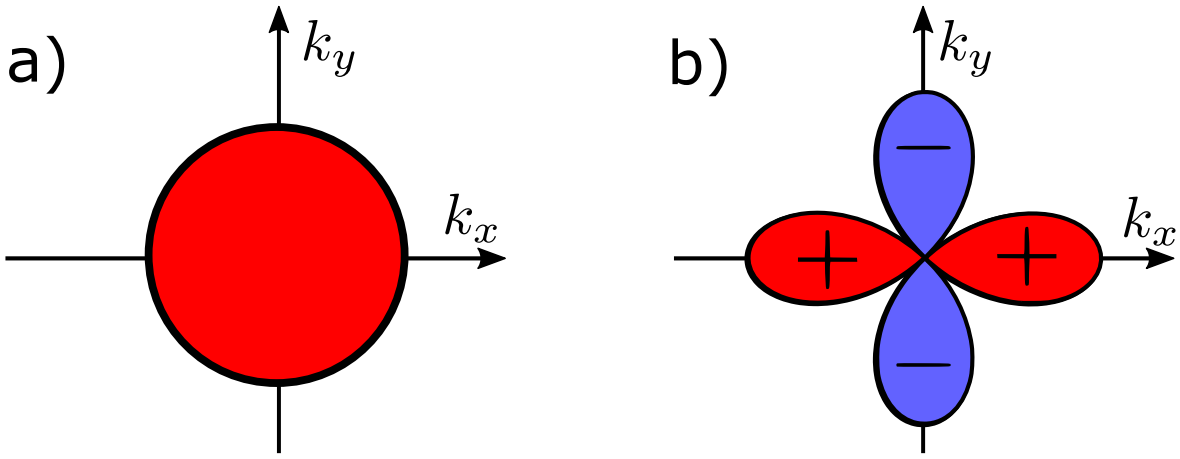

Figure 1.1: *Order parameters in reciprocal space. (a) The uniform s-wave order parameter independent of momentum direction (b) the momentum dependent d-wave order parameter, zero at the nodes.*

Noteworthy, when it comes to unconventional pairing, is also the superfluid He^3 [9, 10].

As the electrons in the superconductors pair, a gap is opened around the Fermi energy. Inside the gap there are no electronic states. The shape of the gap depends on the symmetry of the order parameter. In Figure 1.3 the density of states (DOS) $N(E)$ normalised by the DOS in a normal metal N_F, is plotted. For an s-wave the gap in the DOS is uniform, see Figure 1.3(a) while for a d-wave it will have a v-shape, see Figure 1.3(b). The gap has a v-shape, since the order parameter varies between a maximum and 0 at the nodes where there is no order parameter or gap for that momentum.

1.1.1 Cuprates

One group of HTSCs are the copper oxides, cuprates, discovered in 1986 [12], since then they have attracted immense interest. The cuprate superconductors are layered materials, alternating layers of copper oxides with other metal oxides. In the case of well-known yttrium barium copper oxide (YBCO) [13] those are yttrium and barium. In Figure 1.2 the structure of YBCO is shown, cupper in green form a square lattice sandwiched between yttrium in purple and barium in orange. In all layers there are oxygen in grey. Upon hole

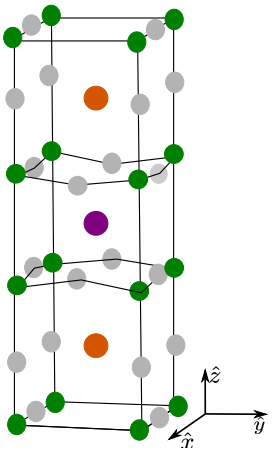

Figure 1.2: *Structure of YBCO with copper in green, oxygen in grey, barium in orange, and yttrium in purple. From [11] with relabelled axes.*

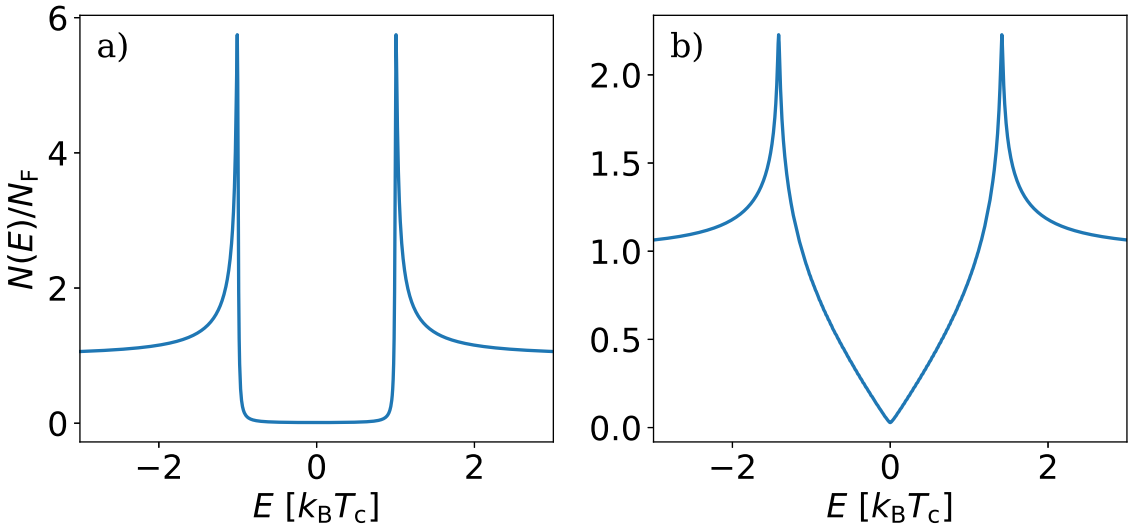

Figure 1.3: *Generic examples of the gap in the density states of superconductor with (a) s-wave and (b) d-wave symmetry. The DOS is on the y-axis normalised by the DOS in a normal metal N_F and the energy, expressed in the units of the Boltzmann factor times transition temperature, is on the x-axis.*

doping the material transition from an antiferromagnetic Mott-insulating state into a superconducting [2]. The superconductivity is believed to take place in the copper-oxide layers and be of *d*-wave symmetry [14, 15].

As mentioned the low temperature part of the phase diagram of cuprates displays an antiferromagnetic region close to half-filling and a dome-shaped superconducting region when doped. These qualitative features have been possible to model using the $t - J$ model [16–20], see also Sections 2.2 and 3 and Figures 4.3(c)-(d).

1.2 Inhomogeneous Cuprates With Strong Electron-Electron Interactions

While, homogeneous properties of cuprates have been quite extensively investigated with the $t - J$ model using the Gutzwiller approximation see for example [16, 18, 20–22] , less has been done for inhomogeneous systems, especially so for systems where superconductivity coexists with antiferromagnetism. Disorder can be introduced into the system via defects [23–26], grain boundaries [27], interfaces [28], vortices [29–31], and edges [32–36]. Of which edges are the focus of the present thesis and especially so the [110] edge, see Figure 5.1. In Reference [36] edges are studied assuming a uniform distribution of electrons. In Reference [34] the edges are studied in a grain system at a doping where antiferromagnetic order

is not expected allowing for redistribution of charge. The results presented in the thesis complement these studies by exploring a larger doping region, including the antiferromagnetic one, and allowing for redistribution of electrons.

1.3 Outline of Thesis

In Chapter 2 the BSC theory is introduced and compared with a weak-coupling mean-field approach to the $t-J$ model. The meaning of the possible symmetries of order parameters on a square lattice is also discussed. In Chapter 3 the Statistically Consistent Gutzwiller approach to the strongly correlated $t-J$ model is presented. Included is a derivation of Gutzwiller factors using counting arguments and fugacity factors. In Chapter 4 the self-consistent equations in a homogeneous system are derived and solved. The phase diagrams and density of states are plotted. The same is done in Chapter 5, but for an inhomogeneous slab including the [110] edge. Finally, in Chapter 6 the reader finds a short summary and suggestions for some possible further aspects to investigate.

2 Modelling Superconductors

Since the discovery of superconductivity many theoretical theories have been developed to describe it. One of these is the Bardeen-Cooper-Schrieffer (BSC) theory which well explains and accurately predicts many properties of conventional superconductors [1]. One model which has been successful in qualitatively capturing aspects of cuprates is the t–J model. In its most strongly correlated formulation, the$t$–J model includes restriction of doubly occupied states. Two strategies to handle the t–J model with these restrictions are Variational Monte Carlo simulations and the Gutzwiller approximation. The focus of the present thesis is the latter.

In Chapter 2 the BSC theory is first introduced followed by a comparison with the t–J model. In Chapter 3 is the Gutzwiller approach more thoroughly outlined. In addition to the microscopic models presented, there are also other theories at longer length scales. Among them the Ginzburg-Landau theory and the quasi-classical theory.

2.1 BCS Theory

The following section is based on [1]. Within the BSC theory, an attractive interaction between electrons, mediated by phonons, is assumed. The interaction makes the electrons form pairs. Forming these pairs lowers the energy and depletes the region around the Fermi energy of electron states, opening up a gap. The physics can be described, in the language of second-quantisation, by

$$H_{\mathrm{BCS}} = \sum_{\boldsymbol{k}\sigma} \xi_{\boldsymbol{k}} \hat{c}^{\dagger}_{\boldsymbol{k}\sigma} \hat{c}_{\boldsymbol{k}\sigma} + \sum_{\boldsymbol{k}\boldsymbol{k}'} V_{\boldsymbol{k}\boldsymbol{k}'} \hat{c}^{\dagger}_{\boldsymbol{k}\uparrow} \hat{c}^{\dagger}_{-\boldsymbol{k}\downarrow} \hat{c}_{-\boldsymbol{k}'\downarrow} \hat{c}_{\boldsymbol{k}'\uparrow}, \tag{2.1}$$

where the first term is the kinetic energy measured relative to the chemical potential μ and the second term gives rise to the pairing. Carrying out at mean-field approximation,

$$\hat{c}^{\dagger}_{i\sigma'} \hat{c}_{i\sigma} \hat{c}^{\dagger}_{j\sigma} \hat{c}_{j\sigma'} \approx \hat{c}^{\dagger}_{i\sigma'} \hat{c}^{\dagger}_{j\sigma} \langle \hat{c}_{i\sigma} \hat{c}_{j\sigma'} \rangle + \langle \hat{c}^{\dagger}_{i\sigma'} \hat{c}^{\dagger}_{j\sigma} \rangle \hat{c}_{i\sigma} \hat{c}_{j\sigma'} - \langle \hat{c}^{\dagger}_{i\sigma'} \hat{c}^{\dagger}_{j\sigma} \rangle \langle \hat{c}_{i\sigma} \hat{c}_{j\sigma'} \rangle \tag{2.2}$$

where the last term is scalar. The Hamiltonian is rewritten in weak-coupling theory, as the mean-field BSC pairing Hamiltonian

$$H^{\mathrm{MF}}_{\mathrm{BCS}} = \sum_{\boldsymbol{k}\sigma} \xi_{\boldsymbol{k}} \hat{c}^{\dagger}_{\boldsymbol{k}\sigma} \hat{c}_{\boldsymbol{k}\sigma} - \sum_{\boldsymbol{k}} {\Delta_{\boldsymbol{k}}}^{*} \hat{c}_{-\boldsymbol{k}\downarrow} \hat{c}_{\boldsymbol{k}\uparrow} - \sum_{\boldsymbol{k}} \Delta_{\boldsymbol{k}} \hat{c}^{\dagger}_{\boldsymbol{k}\uparrow} \hat{c}^{\dagger}_{-\boldsymbol{k}\downarrow} = \hat{C}_{\boldsymbol{k}}{}^{\dagger} H_{\boldsymbol{k}} \hat{C}_{\boldsymbol{k}}, \tag{2.3}$$

where $\Delta_{\boldsymbol{k}} = -\sum_{\boldsymbol{k}'} V_{\boldsymbol{k}\boldsymbol{k}'} \langle \hat{c}_{-\boldsymbol{k}'\downarrow} \hat{c}_{\boldsymbol{k}'\uparrow} \rangle$ is a measure of the strength of the interaction and thereby the gap,

$$\hat{C}_{\boldsymbol{k}} = \begin{pmatrix} \hat{c}_{\boldsymbol{k}\uparrow} \\ \hat{c}^{\dagger}_{-\boldsymbol{k}\downarrow} \end{pmatrix} \tag{2.4}$$

and

$$H_{\boldsymbol{k}} = \begin{pmatrix} \xi_{\boldsymbol{k}} & \Delta_{\boldsymbol{k}} \\ -\Delta_{\boldsymbol{k}}{}^{*} & -\xi_{\boldsymbol{k}} \end{pmatrix}. \tag{2.5}$$

Performing a Bogoliubov rotation the operators may be expressed as

$$\hat{C}_{\boldsymbol{k}} = \begin{pmatrix} \hat{c}_{\boldsymbol{k}\uparrow} \\ \hat{c}^{\dagger}_{-\boldsymbol{k}\downarrow} \end{pmatrix} = \begin{pmatrix} u_{\boldsymbol{k}} & v_{\boldsymbol{k}} \\ v_{\boldsymbol{k}}{}^{*} & u_{\boldsymbol{k}}{}^{*} \end{pmatrix} \begin{pmatrix} \hat{a}_{\boldsymbol{k}} \\ \hat{a}^{\dagger}_{\boldsymbol{k}} \end{pmatrix} = U_{\boldsymbol{k}} \hat{A}_{\boldsymbol{k}} \tag{2.6}$$

where $U_{\boldsymbol{k}}$ is chosen such that it diagonalises $H_{\boldsymbol{k}}$, giving

$$U_{\boldsymbol{k}} = \frac{1}{\sqrt{2E_{\boldsymbol{k}}(E_{\boldsymbol{k}} - \xi_{\boldsymbol{k}})}} \begin{pmatrix} E_{\boldsymbol{k}} + \xi_{\boldsymbol{k}} & \Delta_{\boldsymbol{k}} \\ -\Delta_{\boldsymbol{k}} & E_{\boldsymbol{k}} + \xi_{\boldsymbol{k}} \end{pmatrix} \tag{2.7}$$

where $E_{\boldsymbol{k}} = \pm\sqrt{{\xi_{\boldsymbol{k}}}^2 + |\Delta_{\boldsymbol{k}}|^2}$ are the eigenvalues of $H_{\boldsymbol{k}}$ and the columns are the corresponding eigenvectors. Equipped with this expression of $U_{\boldsymbol{k}}$ the annihilation operators can be expressed using the operators

$$\hat{A}_{\boldsymbol{k}} = \begin{pmatrix} \hat{a}_{\boldsymbol{k}} \\ \hat{a}^{\dagger}_{\boldsymbol{k}} \end{pmatrix} \tag{2.8}$$

which diagonalise the Hamiltonian, are free fermions, and therefore their distribution follow the Fermi-Dirac-distribution function

$$n_F(E_{\boldsymbol{k}}) = \frac{1}{e^{E_{\boldsymbol{k}}\beta} + 1} \tag{2.9}$$

where $\beta = 1/k_B T$ with T the temperature. After the rotation, the Hamiltonian can be written

$$H^{\mathrm{MF}}_{\mathrm{BSC}} = \sum_{\boldsymbol{k}} E_{\boldsymbol{k}} \hat{a}^{\dagger}_{\boldsymbol{k}} \hat{a}_{\boldsymbol{k}} + \text{constant}. \tag{2.10}$$

Continuing by expressing the operators $\hat{C}_{\boldsymbol{k}}$ in $\hat{A}_{\boldsymbol{k}}$ the gap equation follows as

$$\Delta_{\boldsymbol{k}} = \sum_{\boldsymbol{k}'} V_{\boldsymbol{k}\boldsymbol{k}'} \frac{\Delta_{\boldsymbol{k}'}}{2E_{\boldsymbol{k}'}} \tanh E_{\boldsymbol{k}'}\beta \tag{2.11}$$

However, remember that $E_{\boldsymbol{k}}$ depends on Δ why Equation (2.11) needs to be solved self-consistently using iterative methods.

Finally the Density of States (DOS) at an energy ω is given by [37]

$$\mathcal{N}(\omega) = \sum_{\boldsymbol{k}} \left(|u_{\boldsymbol{k}}|^2 \delta(\omega - E_{lk}) + |v_{\boldsymbol{k}}|^2 \delta(\omega + E_{lk}) \right). \tag{2.12}$$

An alternative way to arrive at the same results as above is to assume that the system is described by the variational BSC ground state

$$|\Psi_{\mathrm{BSC}}\rangle = \Pi_{\boldsymbol{k}}(u_{\boldsymbol{k}} + v_{\boldsymbol{k}}\hat{c}^{\dagger}_{\boldsymbol{k}\uparrow}\hat{c}^{\dagger}_{-\boldsymbol{k}\downarrow})|0\rangle, \tag{2.13}$$

where $|0\rangle$ is the vacuum state, $u_{\boldsymbol{k}}$ the amplitude for the pair state $\boldsymbol{k}$ is being empty and $v_{\boldsymbol{k}}$ the amplitude for it being filled. By expressing the energy $\langle\Psi_{\mathrm{BSC}}|H^{\mathrm{MF}}_{\mathrm{BCS}}|\Psi_{\mathrm{BSC}}\rangle$ and minimising it $u_{\boldsymbol{k}}$ and $v_{\boldsymbol{k}}$ can be found. [Bruus Flensberg]

2.2 t–J model

The t–J model was originally derived to explain antiferromagnetism in Mott insulators [38]. The model pictures the atomic orbitals of a material as lattice sites which can be occupied by electrons [17]. Thus, the lattice geometry corresponds to the arrangement of atoms in the material. Between the sites electrons may jump, with hopping amplitude t, and spins interact via exchange interaction with amplitude J. In Figure 2.1 a 2D square lattice with lattice constant d and symmetry axes x and y is shown. The blue arrows represent the spin of electrons occupying the sites, as there are fewer electrons than sites, the example is hole-doped. The pink arrow gives an example of exchange coupling and the black of possible hopping processes. Both take place on links indicated by black lines between sites. Only nearest-neighbour interactions are depicted. The processes may be described by the Hamiltonian

$$\hat{H}_{t\text{–}J} = t\sum_{\langle ij\rangle\sigma}\hat{P}_C(\hat{c}^{\dagger}_{i\sigma}\hat{c}_{j\sigma} + \text{h.c.})\hat{P}_C + J\sum_{\langle ij\rangle}\hat{\boldsymbol{S}}_i\cdot\hat{\boldsymbol{S}}_j, \tag{2.14}$$

which may be derived through a Schrieffer-Wolf transformation from the Hubbard model [39] and where $\hat{\boldsymbol{S}}_i = \sum_\tau \hat{S}^\tau_i$ with $\tau \in \{x, y, z\}$ and the spin component along τ at site i is given by

$$\hat{S}^\tau_i = \begin{pmatrix}\hat{c}^{\dagger}_{i\uparrow} & \hat{c}^{\dagger}_{i\downarrow}\end{pmatrix}\boldsymbol{\sigma}_\tau\begin{pmatrix}\hat{c}_{i\uparrow}\\ \hat{c}_{i\downarrow}\end{pmatrix} \tag{2.15}$$

where $\boldsymbol{\sigma_\tau}$ is the relevant Pauli matrix. So, $\hat{\boldsymbol{S}}_i$ is bilinear in operators and $\hat{\boldsymbol{S}}_i\cdot\hat{\boldsymbol{S}}_j$ consists of four-operator terms. The t–J model may be expanded by considering interactions between more sites, for example including next-nearest neighbours etc. Also completely different terms, such as intersite Coulomb interaction

$$\sum_{ij} V_{ij}\hat{n}_i\hat{n}_j \tag{2.16}$$

may be added [17]. In this chapter a weak-coupling approach to the t–J Hamiltonian will be taken, so at the moment the projection correlators P_C excluding doubly occupied states are not considered, but will be in Chapter 3.

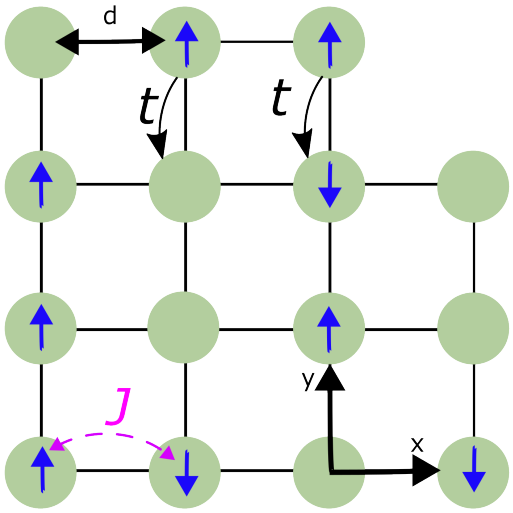

Figure 2.1: *Square lattice where blue arrows at green sites indicate the spins of electrons, t is the hopping amplitude and J the exchange coupling. The black lines indicate links and there are fewer electrons than sites, indicating a hole-doped system. The lattice axes x and y are marked as well as the lattice constant d.*

It is the second term of the t–J Hamiltonian, Equation (2.14), which give rise to the richness of the t–J phase diagram. If J is positive superconductivity and antiferromagnetism (AFM) is preferred, while if negative ferromagnetic order is favoured. Finding the ground state, the same mean-field approximation as before, see Equation (2.2), is once more applied to deal with the four-operator, J, term. Further, for simple expressions, a homogenous lattice with periodic boundary conditions is used and consequently the operators are transformed into reciprocal space according to

$$\hat{c}_{\boldsymbol{k}\sigma} = \frac{1}{\sqrt{N}} \sum_j e^{-i\boldsymbol{k}\cdot\boldsymbol{r}_j} \hat{c}_{j\sigma}, \tag{2.17}$$

where $\boldsymbol{r}_j$ is the position vector of site j and N the total number of sites in the lattice. The mean-field Hamiltonian is in reciprocal space

$$H_{t-J}^{\mathrm{MF}} = \sum_{\boldsymbol{k},\sigma} \xi_{\boldsymbol{k}} (\hat{c}_{\boldsymbol{k}\sigma}^\dagger \hat{c}_{\boldsymbol{k}\sigma} + \mathrm{H.c.}) - \frac{1}{2N} \sum_{\sigma,\boldsymbol{k},\boldsymbol{a}} (\Delta_{\sigma\bar{\sigma},\boldsymbol{k}} + \Delta_{\bar{\sigma}\sigma,\boldsymbol{k}})\, \hat{c}_{\boldsymbol{k}\bar{\sigma}}^\dagger \hat{c}_{-\boldsymbol{k}\sigma}^\dagger + \mathrm{H.c.} \tag{2.18}$$

where

$$\Delta_{\sigma\sigma',\boldsymbol{k}} = \sum_{\boldsymbol{a},\boldsymbol{k}'} J \langle \hat{c}_{\boldsymbol{k}'\sigma} \hat{c}_{-\boldsymbol{k}'\sigma'} \rangle e^{i(\boldsymbol{k}'-\boldsymbol{k})\cdot\boldsymbol{a}} \tag{2.19}$$

with $\boldsymbol{a}$ as the vector between neighbour sites i and j. To find the order parameter and DOS the Hamiltonian is once more diagonalised and the self-consistent equation solved as in Section 2.1

2.2.1 Symmetries on a Square Lattice

The possible space symmetries of the superconducting order parameter depend on the lattice. On a square lattice the vectors connecting nearest neighbours are $\boldsymbol{a} = \{\pm d\hat{\boldsymbol{x}}, \pm d\hat{\boldsymbol{y}}\}$ where the directions $\hat{x}$ and $\hat{y}$ are as indicated in Figure 2.1. Carrying out the sum over vectors gives the factor $\sum_f \cos\left[d(k'_f - k_f)\right]$ where $f \in \{x, y\}$ which expanded using the formula for cosine is

$$\mathcal{Y}_s(\boldsymbol{k})\mathcal{Y}_s(\boldsymbol{k}') + \mathcal{Y}_d(\boldsymbol{k})\mathcal{Y}_d(\boldsymbol{k}') + \mathcal{Y}_{px}(\boldsymbol{k})\mathcal{Y}_{px}(\boldsymbol{k}') + \mathcal{Y}_{py}(\boldsymbol{k})\mathcal{Y}_{py}(\boldsymbol{k}') \tag{2.20}$$

with

$$\begin{cases} \mathcal{Y}_s(\boldsymbol{k}) & = \cos dk_x + \cos dk_y \\ \mathcal{Y}_d(\boldsymbol{k}) & = \cos dk_x - \cos dk_y \\ \mathcal{Y}_{pf}(\boldsymbol{k}) & = \sin dk_f \end{cases} \tag{2.21}$$

where the subscript indicate s-, d- and p-wave symmetry, respectively. It should be pointed out that the s-wave here is more precisely an extended s-wave, but will however in the rest of the thesis be referred to as only s-wave. In real space these symmetries give the relation between the order parameter, or mean-field, on different links see Figure 2.2. In Figure 2.2(a) s-wave symmetry is shown, same sign of the order parameter on all links, in (b) d-wave, the order parameter on y-links have the opposite sign of the order parameter on x-links, in (c) p_x-wave and in (d) p_y-wave the, sign flips between neighbouring links along the x- and y-directions respectively.

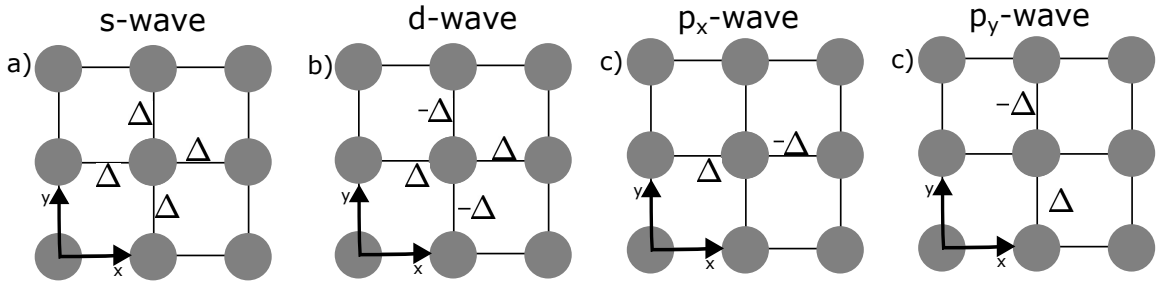

Figure 2.2: *Possible symmetries of the superconductivity on a square lattice in real space. In (a) the s-wave, same order parameter Δ in all directions, is shown, in (b) the d-wave where there is a sign difference between links in the x- and y-direction, in (c) the p_x-wave and in (d) the p_y-wave, the sign of the order parameter is opposite of that on the previous link in the two latter cases.*

The wavefunction of a pair of electron can be viewed as a combination of the space part $\mathcal{Y}(\boldsymbol{r})$ and a spin-part $\chi_{\sigma,\sigma'}$ [2]

$$\Psi(\boldsymbol{r}, \boldsymbol{r}', \sigma, \sigma') = \mathcal{Y}(\boldsymbol{r} - \boldsymbol{r}')\chi_{\sigma,\sigma'}. \tag{2.22}$$

Which in reciprocal space corresponds to

$$\Psi(\boldsymbol{k}, \boldsymbol{k}', \sigma, \sigma') = \mathcal{Y}(\boldsymbol{k} - \boldsymbol{k}')\chi_{\sigma,\sigma'}. \tag{2.23}$$

From the Pauli exclusion principle follows that the wavefunction should be anti-symmetric under exchange of particles, so

$$\Psi(\boldsymbol{r}, \boldsymbol{r}', \sigma, \sigma') = -\Psi(\boldsymbol{r'}, \boldsymbol{r}, \sigma', \sigma). \tag{2.24}$$

By which it follows that either the space-part or the spin-part has to change sign. For s- and d-wave symmetry the space-part has the same sign, thus the spin part needs to change sign which require spin singlet symmetry

$$\frac{1}{\sqrt{2}}(|\uparrow\downarrow\rangle - |\downarrow\uparrow\rangle). \tag{2.25}$$

On the contrary for p-wave symmetry, here the spatial part changes sign and this the spin part cannot, giving triplet symmetry, any or a combination of

$$\begin{cases} |\uparrow\uparrow\rangle, \\ \frac{1}{\sqrt{2}}(|\uparrow\downarrow\rangle + |\downarrow\uparrow\rangle), \\ |\downarrow\downarrow\rangle. \end{cases} \tag{2.26}$$

It is possible to also consider symmetries in time (frequency). In the current thesis even time symmetry is assumed.

3 Gutzwiller Approaches

Here, the restriction of no doubly occupied states is reintroduced in Equation (2.14). The restrictions makes it no longer possible to directly solve this strongly correlated model by directly applying a mean-field approximation and a Bougliobov rotation as in Chapter 2. Instead the Gutzwiller variational ansatz

$$|\Psi_G\rangle = \hat{P}_G|\Psi_0\rangle = \Pi_i \hat{P}_{G,i}|\Psi_0\rangle = \Pi_i(1 - \alpha \hat{n}_{i\uparrow}\hat{n}_{i\downarrow})|\Psi_0\rangle, \tag{3.1}$$

originally proposed in 1962 by Gutzwiller to treat ferromagnetism in metals [40], can be employed. In the ansatz the projected wavefunction $|\Psi_G\rangle$ is related to a single particle wavefunction $|\Psi_0\rangle$ through projection operators $\hat{P}_{G,i}$. The projection operators project out, wholly or partly, doubly occupied states, depending on choice of parameter $\alpha \in [0, 1]$, through this thesis the projection will be chosen to be full ($\alpha = 1$). Expectation values obtained using $|\Psi\rangle_G$ can, for example, be numerically calculated using variational Monte Carlo simulations [16] or by invoking the Gutzwiller approximation [41].

In this Chapter the Gutzwiller approximation will be introduced and the related so called Gutzwiller factors derived. Then it will be shown how the Gutzwiller approximation may be combined with a mean-field approximation to solve the t–J model in the restricted system through a Gutzwiller approach.

3.1 Gutzwiller Factors

Using one variety of the Gutzwiller approximation the expectation value of an operator $\hat{O}$ in the correlated system is related to the uncorrelated system, subscript 0, via a statistical weight (Gutzwiller factor) g^O [19]

$$\langle \hat{O} \rangle = \frac{\langle \Psi|\hat{O}|\Psi\rangle}{\langle \Psi|\Psi\rangle} = \frac{\langle \Psi_0|P_C\hat{O}P_C|\Psi_0\rangle}{\langle \Psi_0|P_CP_C|\Psi_0\rangle} \approx g^O \frac{\langle \Psi_0|\hat{O}|\Psi_0\rangle}{\langle \Psi_0|\Psi_0\rangle} = g^O \langle \hat{O} \rangle_0, \tag{3.2}$$

where the projection operators have been replaced by Gutzwiller correlators, $P_C = \Pi_i \hat{P}_{C,i} = \Pi_i \tilde{\gamma}_i \hat{P}_{G,i}$, including fugacity factors $\tilde{\gamma}$, which are chosen such that the projection conserves electron densities [42]. The conservation can require either the local spin density $\langle \hat{n}_{i\sigma} \rangle = \langle \hat{n}_{i\sigma} \rangle_0$ to be conserved, denoted case I or local electron density conservation $\langle \hat{n}_i \rangle = \langle \hat{n}_i \rangle_0$ denoted case II. Physically, the processes can be seen as either splitting doubly occupied states keeping the occupation and magnetisation, or removing doubly occupied states requiring a

rescaling of all occupations [43]. As will be shown, Gutzwiller factors are different between I and II in a spin-dependent system.

3.1.1 Fugacity Factors

Choosing local spin conservation, case I, corresponding to the grand canonical ensemble [42], the Guztwiller correlator is written

$$P_C = \Pi_i \gamma_{i\uparrow}^{n_{i\uparrow}/2} \gamma_{i\downarrow}^{n_{i\downarrow}/2} \hat{P}_{G,i} \tag{3.3}$$

where γ is found from the constraint $\langle n_{i\sigma} \rangle = \langle n_{i\sigma} \rangle_0 = n_{i\sigma}$, giving the condition

$$\langle \hat{n}_{i\sigma} \rangle = \frac{\langle \hat{n}_{i\sigma} P_{C,i}^2 \Pi_{l\neq i} P_{C,l}^2 \rangle_0}{\langle \Pi_l P_{C,l}^2 \rangle_0} = \frac{\langle \hat{n}_{i\sigma} \gamma_{i\sigma} (1 - \hat{n}_{i\bar{\sigma}}) \Pi_{l\neq i} P_{C,l}^2 \rangle_0}{\langle P_{C,i}^2 \Pi_{l\neq i} P_{C,l}^2 \rangle_0} = \hat{n}_{i\sigma} \tag{3.4}$$

where, since the expectation value is non-zero only if $i\sigma$ is occupied, $j\bar{\sigma}$ is unoccupied, and because $(1 - \hat{n}_{i\bar{\sigma}})^2 = (1 - \hat{n}_{i\bar{\sigma}})$, the squared correlator at site i has been simplified as $P_{C,i}^2 = \gamma_{i\uparrow}^{\hat{n}_{i\uparrow}} \gamma_{i\downarrow}^{\hat{n}_{i\downarrow}} (1 - \hat{n}_{i\uparrow}\hat{n}_{i\downarrow})^2 = \gamma_{i\sigma}(1 - \hat{n}_{i\bar{\sigma}})$. Keeping only on-site contractions the $\Pi_{l\neq i} P_{C,l}^2$ terms cancel [Fukushima, Debmalya Theses], which yields

$$\langle \hat{n}_{i\sigma} \rangle = \frac{\langle \hat{n}_{i\sigma} \gamma_{i\sigma} (1 - \hat{n}_{i\bar{\sigma}}) \rangle_0}{\langle P_{C,i}^2 \rangle_0} = \frac{\gamma_{i\sigma}(1 - n_{i\sigma}) n_{i\sigma}}{\langle P_{C,i}^2 \rangle_0}, \tag{3.5}$$

where

$$\langle P_{C,i}^2 \rangle_0 = (1 - n_{i\uparrow})(1 - n_{i\downarrow}) + \gamma_{i\uparrow} n_{i\uparrow}(1 - n_{i\downarrow}) + \gamma_{i\downarrow} n_{i\downarrow}(1 - n_{i\uparrow}). \tag{3.6}$$

Combining these expressions for both spins an equation system is obtained

$$\begin{cases} \gamma_{i\uparrow} = \frac{\langle P_{C,i}^2 \rangle_0}{(1 - n_{i\uparrow})} \\ \gamma_{i\downarrow} = \frac{\langle P_{C,i}^2 \rangle_0}{(1 - n_{i\downarrow})} \end{cases} \tag{3.7}$$

with the solution

$$\gamma_{i\sigma}^{II} = \frac{1 - n_{i\sigma}}{1 - n_i} \tag{3.8}$$

and

$$\langle P_{C,i}^2 \rangle_0 = \frac{(1 - n_{i\uparrow})(1 - n_{i\downarrow})}{1 - n_i}. \tag{3.9}$$

Instead choosing conserved local occupation, the fugacity factors are spin independent

$$P_C = \Pi_i \gamma_i^{n_i/2} \hat{P}_{G,i}. \tag{3.10}$$

Putting $\langle \hat{n}_i \rangle = \langle \hat{n}_i \rangle_0 = n_i = n_{i\uparrow} + n_{i\downarrow}$ gives, after similar calculations as for local spin conservation,

$$\gamma_i^{II} = \gamma_{i\uparrow}^{II} = \gamma_{i\downarrow}^{II} = \frac{n_i (1 - n_{i\uparrow})(1 - n_{i\downarrow})}{(1 - n_i)(n_i - 2 n_{i\uparrow} n_{i\downarrow})}, \tag{3.11}$$

and unchanged $\langle P_{C,i}^2 \rangle_0$.

3.1.2 Gutzwiller Factors for Pair of Operators

Starting with finding the Gutzwiller factor for hopping, Equation (3.2) is rewritten, taking $\hat{O} = \hat{c}^\dagger_{i\sigma}\hat{c}_{j\sigma}$, as

$$\begin{aligned} g^t_{ijs} &= \frac{\langle\Psi|\hat{c}^\dagger_{i\sigma}\hat{c}_{j\sigma}|\Psi\rangle}{\langle\Psi|\Psi\rangle} \cdot \frac{\langle\Psi_0|\Psi_0\rangle}{\langle\Psi_0|\hat{c}^\dagger_{i\sigma}\hat{c}_{j\sigma}|\Psi_0\rangle} \\ &= \frac{\langle\Psi|(1-\hat{n}_{i\bar{\sigma}})\hat{c}^\dagger_{i\sigma}\hat{c}_{j\sigma}(1-\hat{n}_{j\bar{\sigma}})|\Psi\rangle}{\langle\Psi|\Psi\rangle} \cdot \frac{(1-n_{i\bar{\sigma}})(1-n_{j\bar{\sigma}})}{\langle\Psi_0|(1-\hat{n}_{i\bar{\sigma}})\hat{c}^\dagger_{i\sigma}\hat{c}_{j\sigma}(1-\hat{n}_{j\bar{\sigma}})|\Psi_0\rangle}, \end{aligned} \tag{3.12}$$

where $(1-\hat{n}_{i\bar{\sigma}})(1-\hat{n}_{j\bar{\sigma}})$ has been introduced in both expectation values to ensure agreement with the infinite dimensions approach [19]. Multiplication by the operator term does not change the expectation value in the correlated state, but does change the uncorrelated with a factor $(1-n_{i\bar{\sigma}})(1-n_{j\bar{\sigma}})$. To compensate, the same factor has been multiplied, and appears in the numerator. Further, the uncorrelated state is constructed such that $\langle\Psi_0|\Psi_0\rangle = 1$.

The first factor in Equation (3.12) is then written out including the Gutzwiller correlators, Ã‰quation (3.3). Keeping only on-site contractions, which will not be stated explicitly in the rest of the chapter, it is seen the correlators cancel for all sites but i and j. Then remain

$$\frac{\langle\Psi_0|\gamma^{n_{i\uparrow}}_{i\uparrow}\gamma^{n_{i\downarrow}}_{i\downarrow}\gamma^{n_{j\uparrow}}_{j\uparrow}\gamma^{n_{j\downarrow}}_{j\downarrow}(1-\hat{n}_{i\bar{\sigma}})(1-\hat{n}_{i\sigma}\hat{n}_{i\bar{\sigma}})\hat{c}^\dagger_{i\sigma}\hat{c}_{j\sigma}(1-\hat{n}_{j\bar{\sigma}})(1-\hat{n}_{j\sigma}\hat{n}_{j\bar{\sigma}})|\Psi_0\rangle}{\langle P^2_{C,i}P^2_{C,j}\rangle_0}.$$

The ket-part is non zero when $j\sigma$ is occupied, $\hat{n}_{j\sigma} = 1$, and $i\sigma$ empty, gives contribution $\sqrt{(1-n_{i\sigma})n_{j\sigma}(1-n_{i\bar{\sigma}})(1-n_{j\bar{\sigma}})\gamma_{j\sigma}}$, the bra-part is non zero when $i\sigma$ is occupied and $j\sigma$ empty, contributes $\sqrt{(1-n_{j\sigma})n_{i\sigma}(1-n_{i\bar{\sigma}})(1-n_{j\bar{\sigma}})\gamma_{i\sigma}}$ the square root coming from the contributions being amplitudes [Edegger]. Considering the same expectation value in the uncorrelated state

$$\langle\Psi|(1-\hat{n}_{i\bar{\sigma}})\hat{c}^\dagger_{i\sigma}\hat{c}_{j\sigma}(1-\hat{n}_{j\bar{\sigma}})|\Psi\rangle_0$$

the ket-part contributes $\sqrt{(1-n_{i\bar{\sigma}})(1-n_{j\sigma})n_{i\sigma}(1-n_{j\bar{\sigma}})}$ and the bra-part $\sqrt{(1-n_{i\bar{\sigma}})(1-n_{i\sigma})n_{j\sigma}(1-n_{j\bar{\sigma}})}$. Put into Equation (3.12) it gives

$$g^t_{ij\sigma} = \frac{(1-n_{i\bar{\sigma}})(1-n_{j\bar{\sigma}})\sqrt{\gamma_{i\sigma}\gamma_{j\sigma}}}{\langle P^2_{C,i}\rangle_0\langle P^2_{C,j}\rangle_0}. \tag{3.13}$$

Consequently with spin conservation the final factor is

$$g^{t,I}_{ij\sigma} = \sqrt{\frac{1-n_i}{1-n_{i\sigma}}}\sqrt{\frac{1-n_j}{1-n_{j\sigma}}}. \tag{3.14}$$

and with occupation conservation

$$g_{ij\sigma}^{t,II} = \sqrt{\frac{n_i(1-n_i)(1-n_{i\bar{\sigma}})}{(1-n_{i\sigma})(n_i-2n_{i\uparrow}n_{i\downarrow})}}\sqrt{\frac{n_j(1-n_j)(1-n_{j\bar{\sigma}})}{(1-n_{j\sigma})(n_j-2n_{j\uparrow}n_{j\downarrow})}}. \tag{3.15}$$

In the non-antiferromagnetic case, $n_{i\uparrow} = n_{i\downarrow} = n/2$, there is no difference between the Gutzwiller factors and they reduce to

$$g_{ij}^{t} = 2\sqrt{\frac{1-n_i}{2-n_i}}\sqrt{\frac{1-n_j}{1-n_j}} = 2\frac{1-n}{2-n}. \tag{3.16}$$

where the last equality holds for homogeneous systems $n_i = n$.

Similar calculations can be carried out for other relevant expectation values. For superconductivity, $\hat{O} = \hat{c}_{i\bar{\sigma}}^{\dagger}\hat{c}_{j\sigma}$

$$g_{ij\sigma}^{\Delta} = \frac{(1-n_{i\sigma})(1-n_{j\bar{\sigma}})\sqrt{\gamma_{i\bar{\sigma}}\gamma_{j\sigma}}}{\langle P_{C,i}^2\rangle_0\langle P_{C,j}^2\rangle_0}, \tag{3.17}$$

which differs from g^t due to the operator-pair having opposite spin and not the same as for hopping. The two cases written out are

$$g_{ij\sigma}^{\Delta,I} = \sqrt{\frac{1-n_i}{1-n_{i\bar{\sigma}}}}\sqrt{\frac{1-n_j}{1-n_{j\sigma}}}. \tag{3.18}$$

and

$$g_{ij\sigma}^{\Delta,II} = \sqrt{\frac{n_i(1-n_i)(1-n_{i\sigma})}{(1-n_{i\bar{\sigma}})(n_i-2n_{i\uparrow}n_{i\downarrow})}}\sqrt{\frac{n_j(1-n_j)(1-n_{j\bar{\sigma}})}{(1-n_{j\sigma})(n_j-2n_{j\uparrow}n_{j\downarrow})}}. \tag{3.19}$$

In the non-antiferromagnetic case, they are the same as for hopping $g_{ij}^{\Delta} = g_{ij}^{t}$.

By definition, there is no Gutzwiller factor for magnetisation in the case of local spin conservation since

$$\langle m_i\rangle = \langle n_{i\uparrow}\rangle - \langle n_{i\downarrow}\rangle = n_{i\uparrow} - n_{i\downarrow} = \langle m_i\rangle_0, \tag{3.20}$$

but when relaxed into occupation conservation there is, and it is given by

$$g_i^{m,II} = \frac{\gamma_i}{\langle P_{C,i}^2\rangle_0} = \frac{n_i}{n_i - 2n_{i\uparrow}n_{i\downarrow}}. \tag{3.21}$$

3.1.3 Gutzwiller Factor for Four-Operator Terms

The Gutzwiller factors related to the four-operator terms arising from the exchange coupling term are treated similarly with some slight adjustments. The

exchange coupling term is expanded as, see Equation (2.15)

$$\begin{aligned}\langle \hat{\boldsymbol{S}}_i \cdot \hat{\boldsymbol{S}}_j \rangle &= \langle \hat{S}_i^x \hat{S}_j^x \rangle + \langle \hat{S}_i^y \hat{S}_j^y \rangle + \langle \hat{S}_i^z \hat{S}_j^z \rangle \\ &= \frac{1}{2} \sum_{\sigma} \langle \hat{c}_{i\bar{\sigma}}^\dagger \hat{c}_{i\sigma} \hat{c}_{j\sigma}^\dagger \hat{c}_{j\bar{\sigma}} \rangle + \frac{1}{4} \sum_{\sigma,\sigma'} \Xi_\sigma \Xi_{\sigma'} \langle \hat{c}_{i\sigma}^\dagger \hat{c}_{i\sigma} \hat{c}_{j\sigma'}^\dagger \hat{c}_{j\sigma'} \rangle .\end{aligned} \tag{3.22}$$

The first two terms, first term in the last row, are related to spin along the x- and y-spin axes also labelled in-plane. The last term is related to spin along the z-axis, out-of-plane.

The Gutzwiller factor for the first term, xy-term, is

$$g_{xy}^J = \frac{\langle \Psi | \hat{c}_{i\bar{\sigma}}^\dagger \hat{c}_{i\sigma} \hat{c}_{j\sigma}^\dagger \hat{c}_{j\bar{\sigma}} | \Psi \rangle}{\langle \Psi | \Psi \rangle} \cdot \frac{1}{\langle \Psi_0 | \hat{c}_{i\bar{\sigma}}^\dagger \hat{c}_{i\sigma} \hat{c}_{j\sigma}^\dagger \hat{c}_{j\bar{\sigma}} | \Psi_0 \rangle}. \tag{3.23}$$

Note, that the factors $(1 - n_{i\bar{\sigma}})$ do not need to be explicitly introduced since they automatically follow from the operators. The ket-part is non-zero if $j\bar{\sigma}$ and $i\sigma$ are occupied and $j\sigma$ and $i\bar{\sigma}$ are empty. The bra-part is non-zero if the opposite is true, giving contributions: $\sqrt{n_{i\sigma} n_{i\bar{\sigma}} n_{j\sigma} n_{j\bar{\sigma}} (1 - n_{i\sigma})(1 - n_{i\bar{\sigma}})(1 - n_{j\sigma})(1 - n_{j\bar{\sigma}})}$ and $\sqrt{\gamma_{i\sigma}\gamma_{i\bar{\sigma}}\gamma_{j\sigma}\gamma_{j\bar{\sigma}} n_{i\sigma} n_{i\bar{\sigma}} n_{j\sigma} n_{j\bar{\sigma}} (1 - n_{i\sigma})(1 - n_{i\bar{\sigma}})(1 - n_{j\sigma})(1 - n_{j\bar{\sigma}})}$ so

$$g_{xy}^J = \frac{\sqrt{\gamma_{i\sigma}\gamma_{i\bar{\sigma}}\gamma_{j\sigma}\gamma_{j\bar{\sigma}}}}{\langle P_{\mathrm{C},i}^2 \rangle \langle P_{\mathrm{C},j}^2 \rangle} \tag{3.24}$$

which in the case of local spin conservation is

$$g_{xy}^{J,I} = \frac{1}{\sqrt{(1 - n_{i\uparrow})(1 - n_{i\downarrow})(1 - n_{j\uparrow})(1 - n_{j\downarrow})}} \tag{3.25}$$

and in the case of local occupation conservation

$$g_{xy}^{J,II} = \frac{n_i n_j}{(n_i - 2n_{i\uparrow} n_{i\downarrow})(n_j - 2n_{j\uparrow} n_{j\downarrow})}, \tag{3.26}$$

which both reduce to

$$g_{xy}^J = \frac{4}{(2 - n_i)(2 - n_j)} \tag{3.27}$$

in a spin independent case.

The second term, z-term, comes with the Gutzwiller factor

$$g_z^J = \frac{\langle \Psi | \hat{c}_{i\sigma}^\dagger \hat{c}_{i\sigma} (1 - n_{i\bar{\sigma}}) \hat{c}_{j\sigma'}^\dagger \hat{c}_{j\sigma'} (1 - n_{j\bar{\sigma}'}) | \Psi \rangle}{\langle \Psi | \Psi \rangle} \cdot \frac{(1 - n_{i\bar{\sigma}})(1 - n_{j\bar{\sigma}'})}{\langle \Psi | \hat{c}_{i\sigma}^\dagger \hat{c}_{i\sigma} (1 - n_{i\bar{\sigma}}) \hat{c}_{j\sigma'}^\dagger \hat{c}_{j\sigma'} (1 - n_{j\bar{\sigma}'}) | \Psi \rangle}. \tag{3.28}$$

the ket-part is non-zero if $i\sigma$ and $j\sigma'$ are occupied and $i\bar{\sigma}$ and $j\bar{\sigma}'$ empty. The same holds for the bra-part, leaving contributions $n_{i\sigma}n_{j\sigma'}(1-n_{i\bar{\sigma}})(1-n_{j\bar{\sigma}'})$ and $\gamma_{i\sigma}\gamma_{j\sigma'}n_{i\sigma}n_{j\sigma'}(1-n_{i\bar{\sigma}})(1-n_{j\bar{\sigma}'})$ so

$$g_z^J = \frac{\gamma_{i\sigma}\gamma_{j\sigma'}(1-n_{i\bar{\sigma}})(1-n_{j\bar{\sigma}'})}{\langle P_{C,i}^2\rangle\langle P_{C,j}^2\rangle} \tag{3.29}$$

which with local spin conservations is

$$g_z^J = 1 \tag{3.30}$$

and with local occupation conservation

$$g_z^J = \frac{n_i n_j}{(n_i - 2n_{i\uparrow}n_{i\downarrow})(n_j - 2n_{j\uparrow}n_{j\downarrow})}. \tag{3.31}$$

For the used derivation scheme the Gutzwiller approximation is thus not always preserving rotational symmetry. In case I it can be understood from the fact that only taking on-site contractions into considerations the z-term can be written

$$\langle \hat{S}_i^z \hat{S}_j^z\rangle = \langle m_i\rangle\langle m_j\rangle \tag{3.32}$$

which is by the construction of the fugacity factors said to be conserved. The assumption of local spin conservation demands the selection of a spin axis, which inherently breaks rotational symmetry. Sometimes the same factor is however taken for $\langle \hat{S}_i^z \hat{S}_j^z\rangle$ as $\langle \hat{S}_i^x \hat{S}_j^x\rangle$ and $\langle \hat{S}_i^y \hat{S}_j^y\rangle$to avoid breaking the symmetry due to form of the Gutzwiller factors, see also [44, 45]. Finally, it should be noted that the Gutzwiller factors will be different if more contractions are kept in the derivation, see for exampled [18, 42].

3.2 Mean-Field Guztwiller Approaches

The Gutzwiller wavefunction can also be used to approach the strongly correlated t–J model. Within the subgroup of mean-field approaches the aim is to minimise the energy [16, 18, 20, 25, 34]. In early works [16] this was done by renormalising the t–J Hamiltonian, Equation (2.14), giving an effective Hamiltonian

$$\hat{H}_{\text{eff}} = t\sum_{\langle ij\rangle\sigma}(g_{ij}^t \hat{c}_{i\sigma}^\dagger \hat{c}_{j\sigma} + \text{h.c.}) + J\sum_{\langle ij\rangle} g_{ij}^s \hat{\boldsymbol{S}}_i \cdot \hat{\boldsymbol{S}}_j, \tag{3.33}$$

and subsequently solve it with a mean-field decoupling and Bougoliobov rotation as in Section 2.2. Over time more involved approaches have developed, which instead of working directly with the effective Hamiltonian Equation (3.33) form a Hamiltonian using the expectation value of the energy

$$W = \langle \hat{H}_{\text{eff}}\rangle_0, \tag{3.34}$$

which is explicitly calculated for the homogenous case in Equation (4.18) and inhomogeneous in (5.4). In one approach, sometimes called Renormalised Mean Field Theory (RMFT) [46], constraints are added to the energy to ensure fixed total occupation $\sum_i n_i = N$ and normalisation of the wavefunction $\langle\Psi_0|\Psi_0\rangle = 1$ [25] giving

$$\tilde{W} = W - \lambda(1 - \langle\Psi_0|\Psi_0\rangle) - \mu\sum_i (n_i - N). \tag{3.35}$$

The Hamiltonian is then formed taking the derivatives of the energy with added constraints with respect to the considered mean-fields

$$\hat{H}_{\mathrm{RMFT}} = \sum_{ij\sigma} \frac{\partial\tilde{W}}{\partial\chi_{ij\sigma}} \hat{c}^\dagger_{i\sigma}\hat{c}_{j\sigma} + \mathrm{H.c.} + \sum_{ij\sigma} \frac{\partial\tilde{W}}{\partial\Delta_{ij\sigma}} \Xi_\sigma \hat{c}_{i\sigma}\hat{c}_{j\bar{\sigma}} + \mathrm{H.c.} + \sum_{i\sigma} \frac{\partial\tilde{W}}{\partial n_{i\sigma}} \hat{c}^\dagger_{i\sigma}\hat{c}_{i\sigma} \tag{3.36}$$

where $\Xi_\uparrow = 1$ and $\Xi_\downarrow = -1$ and

$$\begin{aligned} \chi_{ij\sigma} &= \langle\hat{c}^\dagger_{i\sigma}\hat{c}_{j\sigma}\rangle_0, \\ \Delta_{ij\sigma} &= \langle\hat{c}_{i\bar{\sigma}}\hat{c}_{j\sigma}\rangle_0, \\ n_{i\sigma} &= \langle\hat{c}^\dagger_{i\sigma}\hat{c}_{i\sigma}\rangle_0. \end{aligned} \tag{3.37}$$

The Hamiltonian is then solved using a Bouglibov transformation. See also for example [34] where a slightly different $\tilde{W}$ is employed.

In this thesis the Statistical Consistent Gutzwiller Approach (SGA) will be used [20–22, 47]. The RMFT and SGA approaches have been shown to agree in a superconducting state [48]. Using the SGA constraints for all mean-fields are added to the expectation values of the effective Hamiltonian to ensure that the mean-fields obtained by a self-consistent approach are the same as for variational minimisation [20]. This condition might otherwise be spoiled by the dependence of the Gutzwiller factors on the mean-fields. The constraints are added via Lagrange multipliers λ one for each mean-field, whose symmetry they follow. The mean-field Hamiltonian with added constraints is

$$\begin{aligned} \hat{H}_{\mathrm{SGA}} = W - \sum_{\langle ij\rangle\sigma} &[\lambda^\chi_{ij\sigma}(\hat{c}^\dagger_{i\sigma}\hat{c}_{j\sigma} - \chi_{ijs}) + \lambda^\Delta_{ij\sigma}(\hat{c}_{i\sigma}\hat{c}_{j\bar{\sigma}} - \Delta_{ij\sigma}) + H.c.] \\ &- \sum_{i\sigma}[\lambda^n_{i\sigma}(\hat{n}_{i\sigma} - n_{i\sigma}) + \mu\hat{n}_{i\sigma}] = W + \lambda + \hat{\Psi}^\dagger \boldsymbol{H}\hat{\Psi}, \end{aligned} \tag{3.38}$$

where the scalar terms containing the Lagrange multipliers are collected in λ and the operators have been written in matrix form $\hat{\Psi}^\dagger\boldsymbol{H}\hat{\Psi}$. The Hamiltonian $\boldsymbol{H}$ can be diagonalised by which the eigenvalues E_l and the eigenvectors forming a new basis are calculated. The grand potential functional follows as

$$\Omega = -\frac{1}{\beta}\ln\mathrm{Tr}(e^{-\beta\hat{H}_{\mathrm{SGA}}}) = W + \lambda - \sum_l \ln\left(1 + e^{-\beta E_l}\right) \tag{3.39}$$

at inverse temperature $\beta = 1/k_{\mathrm{B}}T > 0$. The potential is minimised putting the derivatives with respect to mean-fields (A) and Lagrange multipliers (B), to zero. This approach results in equations of the form

$$\begin{aligned} \frac{\partial \Omega}{\partial A} &= \frac{\partial W}{\partial A} + \frac{\partial \lambda}{\partial A} = 0 \\ \frac{\partial \Omega}{\partial B} &= \frac{\partial \lambda}{\partial B} + \sum_l f(E_l) \frac{\partial E_l}{\partial B} = 0. \end{aligned} \tag{3.40}$$

Note that λ is linear in both mean-fields and Lagrange multipliers, see Equation (3.38) which for example contains $\lambda^{\chi}_{ij\sigma}\chi_{ij\sigma}$. The first equation thus gives expressions for Lagrange multipliers and the second self-consistent equations for the mean-fields.

It should be pointed out that the mean-fields are evaluated in the uncorrelated state. The corresponding field in the correlated state is given by multiplication by the appropriate Gutzwiller factor, see Section 3.1. In the case of superconductivity, the superconducting order parameter is given by

$$\Delta^{\mathrm{sc}}_{ij\sigma} = g^{\Delta}_{ij\sigma}\Delta_{ij\sigma}. \tag{3.41}$$

The correlated mean-fields for hopping and antiferromagnetisation are given in the same way, while the fugacity factors ensure that the occupations are the same in the correlated as uncorrelated system.

4 Homogenous Case

To better understand results of inhomogeneous systems, the Statistical Consistent Gutzwiller Approach (SGA) [20–22, 43] is first studied in the homogeneous case. Then the lattice is infinite and without edges, which allows for a study in reciprocal space. First, general equations are derived in a similar fashion as for cases with edges, to make comparisons easier. Second, appropriate simplifications are applied and the phase diagram and the density of states are calculated and presented.

4.1 Evaluation of Mean-Field Hamiltonian

The aim of this section is to compute the grand potential functional Equation (3.39), in doing so the expectation value of the Hamiltonian $W = \langle \hat{H}_{\text{eff}} \rangle_0$ must be calculated and the Hamiltonian $\boldsymbol{H}$ in Equation (3.38) diagonalised. For the evaluation the magnetic unit cell, see Figure 4.1, with two sublattices A and B, thus allowing for antiferromagnetism, is used. Further, the following spin dependent mean-fields are considered

$$\begin{aligned} \chi^f_{ij\sigma} &= \langle \hat{c}^\dagger_{i\sigma} \hat{c}_{j\sigma} \rangle_0 = (\chi^f_{ji\sigma})^*, \\ \Delta^f_{ij\sigma} &= \langle \hat{c}_{i\bar{\sigma}} \hat{c}_{j\sigma} \rangle_0 = -\Delta^f_{ji\bar{\sigma}}, \\ n_{i\sigma} &= \langle \hat{c}^\dagger_{i\sigma} \hat{c}_{i\sigma} \rangle_0, \end{aligned} \tag{4.1}$$

where $f \in \{x, y\}$ dependent on which direction the link lies in. In every unit cell (UC), there are one A site and one B site, each with four neighbours, so consequently there are totally four links in the UC. On the links lie the hopping mean-field, sometimes called bond order, $\chi^f_{ij\sigma}$ and pairing mean-fields Δ^f_{ij}. The links can be in either x- or y-direction, in the case of pairing mean-fields these need to be differentiated to allow for both s- and d-wave symmetry of the order parameter. Computing the occupation densities for spins separately, allows for magnetism $m = n_{i\uparrow} - n_{i\downarrow}$.

To evaluate the sums, all nearest neighbours are summed over. Note that in the sum $\sum_{\langle ij \rangle}$ in Equation (3.38), each link should be counted only once. One unit cell thus leaves the contribution to the hopping term

$$\sum_{\substack{\text{UC} \\ \sigma}} t_{ij\sigma} g^t_{ij\sigma} \langle \hat{c}^\dagger_{i\sigma} \hat{c}_{j\sigma} + \text{H.C.} \rangle_0 = 2 \sum_{\sigma f} t_{f\sigma} g^t_{AB\sigma} [\chi^f_{AB\sigma} + (\chi^f_{AB\sigma})^*], \tag{4.2}$$

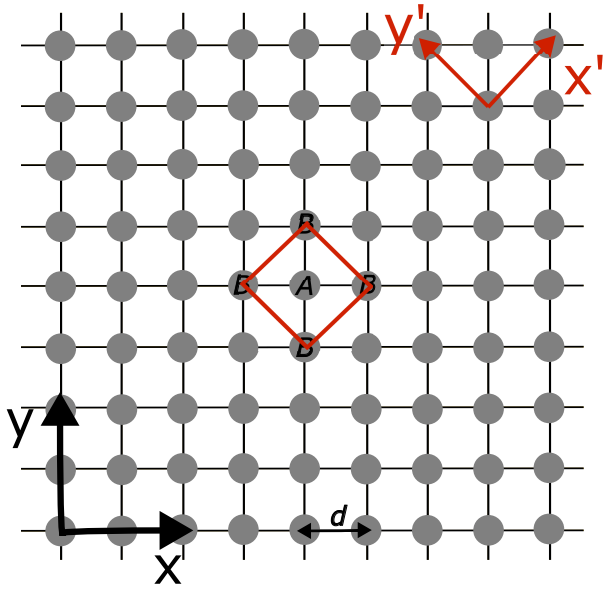

Figure 4.1: *A homogeneous lattice with the magnetic unit cell marked with red lines. The cell contains one A-site in the center and one B-site. The latter in the form of four quarters of neighbouring B-sites, placed in the corners of the unit cell. The lattice constant d, and the x- and y-axes are marked as well as the symmetry axes in reciprocal space x' and y'.*

where $f \in \{x, y\}$. In a lattice of N sites there are are N/2 unit cells, giving a total energy contribution of

$$N \sum_{\sigma f} t_{f\sigma} g^t_{AB\sigma} [\chi^f_{AB\sigma} + (\chi^f_{AB\sigma})^*]. \tag{4.3}$$

In the rest of the chapter, the sum over unit cells and lattice will be calculated in one step.

The exchange term is less straightforward to evaluate, since it consists of four-operator terms, see Equation (2.15). Applying Wicks theorem and the mean-field approximation the terms can be expanded

$$\begin{aligned} \langle \hat{c}^\dagger_{i\sigma'} \hat{c}_{i\sigma} \hat{c}^\dagger_{j\sigma} \hat{c}_{j\sigma'} \rangle_0 \approx & \langle \hat{c}^\dagger_{i\sigma'} \hat{c}_{i\sigma} \rangle_0 \langle \hat{c}^\dagger_{j\sigma} \hat{c}_{j\sigma'} \rangle_0 \\ & - \langle \hat{c}^\dagger_{i\sigma'} \hat{c}^\dagger_{j\sigma} \rangle_0 \langle \hat{c}_{i\sigma} \hat{c}_{j\sigma'} \rangle_0 - \langle \hat{c}^\dagger_{i\sigma'} \hat{c}_{j\sigma'} \rangle_0 \langle \hat{c}_{i\sigma} \hat{c}^\dagger_{j\sigma} \rangle_0, \end{aligned} \tag{4.4}$$

note that more terms are kept compared to the previous mean-field approximation Equation (2.2). The exchange term gives, with $m_i = n_{i\uparrow} - n_{i\downarrow}$, after summing over the lattice the energy contribution

$$\begin{aligned} \sum_{\langle ij \rangle} J_{ij} g^J_{ij} \langle \boldsymbol{S_i} \cdot \boldsymbol{S_j} \rangle_0 = & N \frac{1}{4} g^J_{AB} \sum_f J_f [2 m_A m_B + \sum_\sigma (2 (\Delta^f_{AB\bar{\sigma}})^* \Delta^f_{AB\sigma} \\ & - 2 (\chi^f_{AB\bar{\sigma}})^* \chi^f_{AB\sigma} - |\chi^f_{AB\sigma}|^2 - |\Delta^f_{AB\sigma}|^2)]. \end{aligned} \tag{4.5}$$

Equations 4.3 and (4.5) form W.

Evaluating the sums over mean-fields times Lagrange multipliers, resulting in scalars, gives

$$\tilde{\lambda} = \frac{N}{2}\sum_{\sigma f}\left(2\lambda^{\chi^f}_{AB\sigma}\chi^f_{AB\sigma} + \text{H.C.} + 2\lambda^{\Delta^f}_{AB\sigma}\Delta^f_{AB\sigma} + \text{H.C.} + \lambda_{A\sigma}n_{A\sigma} + \lambda_{B\sigma}n_{B\sigma}\right). \tag{4.6}$$

Further, the operators are transformed according to

$$\begin{aligned}\hat{c}_{j\sigma} =& \frac{1}{\sqrt{N}}\sum_{\boldsymbol{k}}\hat{c}_{\boldsymbol{k}\sigma}e^{i\boldsymbol{k}\boldsymbol{r}_j},\\ \hat{c}^\dagger_{j\sigma} =& \frac{1}{\sqrt{N}}\sum_{\boldsymbol{k}}\hat{c}^\dagger_{\boldsymbol{k}\sigma}e^{-i\boldsymbol{k}\boldsymbol{r}_j},\end{aligned} \tag{4.7}$$

where, using the magnetic unit cell, $\boldsymbol{k} \in (-1/(d\sqrt{2}), 1/d\sqrt{2}]$. The operator terms after transformation are written

$$\begin{aligned}\sum_{\boldsymbol{k}}\hat{\Psi}^\dagger_{\boldsymbol{k}}\boldsymbol{H}_{\boldsymbol{k}}\hat{\Psi}_{\boldsymbol{k}} =& -\sum_{\boldsymbol{k}\sigma}(\lambda^n_{\sigma A}\hat{c}^\dagger_{A\boldsymbol{k}\sigma}\hat{c}_{A\boldsymbol{k}\sigma} + \lambda^n_{\sigma B}\hat{c}^\dagger_{B\boldsymbol{k}\sigma}\hat{c}_{B\boldsymbol{k}\sigma})\\ &- \sum_{\boldsymbol{k}\sigma f}[\lambda^{\chi^f}_{AB\sigma} + (\lambda^{\chi^f}_{AB\sigma})^*]\cos\frac{d(k_x+\Xi_f k_y)}{\sqrt{2}}(\hat{c}^\dagger_{A\boldsymbol{k}\sigma}\hat{c}_{B\boldsymbol{k}\sigma} + \hat{c}^\dagger_{B\boldsymbol{k}\sigma}\hat{c}_{A\boldsymbol{k}\sigma})\\ &- 2\sum_{\boldsymbol{k}\sigma}\lambda^{\Delta^f}_{AB\sigma}\cos\frac{d(k_x+\Xi_f k_y)}{\sqrt{2}}\hat{c}_{A\boldsymbol{k}\sigma}\hat{c}_{B-\boldsymbol{k}\bar{\sigma}} + \text{H.C.},\end{aligned} \tag{4.8}$$

where $\Xi_x = -1$ and $\Xi_y = 1$,

$$\hat{\Psi}_{\boldsymbol{k}} = \begin{pmatrix}\hat{c}_{A\boldsymbol{k}\uparrow}\\ \hat{c}^\dagger_{-A\boldsymbol{k}\downarrow}\\ \hat{c}_{B\boldsymbol{k}\uparrow}\\ \hat{c}^\dagger_{-B\boldsymbol{k}\downarrow}\end{pmatrix}, \tag{4.9}$$

and

$$\boldsymbol{H}_{\boldsymbol{k}} = \begin{pmatrix}-\lambda^n_{A\uparrow}-\mu & 0 & -\zeta_{AB\uparrow\boldsymbol{k}} & \eta^*_{AB\uparrow\boldsymbol{k}}\\ 0 & \lambda^n_{A\downarrow}+\mu & -\eta_{AB\downarrow\boldsymbol{k}} & \zeta_{AB\downarrow\boldsymbol{k}}\\ -\zeta_{AB\uparrow\boldsymbol{k}} & -\eta^*_{AB\downarrow\boldsymbol{k}} & -\lambda^n_{B\uparrow}-\mu & 0\\ \eta_{AB\uparrow\boldsymbol{k}} & \zeta_{AB\downarrow\boldsymbol{k}} & 0 & \lambda^n_{B\downarrow}+\mu\end{pmatrix}, \tag{4.10}$$

with

$$\begin{aligned}\zeta_{AB\sigma\boldsymbol{k}} &= 2\text{Re}[\lambda^{\chi^x}_{AB\sigma}]\cos\frac{d(k_x-k_y)}{\sqrt{2}} + 2\text{Re}[\lambda^{\chi^y}_{AB\sigma}]\cos\frac{d(k_x+k_y)}{\sqrt{2}},\\ \eta_{AB\sigma\boldsymbol{k}} &= 2\lambda^{\Delta^x}_{AB\sigma}\cos\frac{d(k_x-k_y)}{\sqrt{2}} + 2\lambda^{\Delta^y}_{AB\sigma}\cos\frac{d(k_x+k_y)}{\sqrt{2}}.\end{aligned} \tag{4.11}$$

Note that the order of the pair of operators with spin down have been interchanged, giving the additional term, $(\lambda_{A\downarrow} + \lambda_{B\downarrow})/2 + \mu$, why

$$\lambda = \tilde{\lambda} + \frac{\lambda_{A\downarrow} + \lambda_{B\downarrow}}{2} + \mu. \tag{4.12}$$

Focus is then turned to the diagonalisation of the Hamiltonian in Equation (4.10). The diagonalisation is made by a Bogoliubov transformation [37] writing

$$\boldsymbol{H_k} = U_{\boldsymbol{k}}^{\dagger} D_{\boldsymbol{k}} U_{\boldsymbol{k}} \tag{4.13}$$

where $D_{\boldsymbol{k}}$ is a matrix with the eigenvalues $E_{l_{\boldsymbol{k}}}$ of $\boldsymbol{H_k}$ on the diagonal, and

$$U_{\boldsymbol{k}} = \begin{pmatrix} u_{A1\boldsymbol{k}\uparrow} & u_{A2\boldsymbol{k}\uparrow} & v_{A1\boldsymbol{k}\uparrow} & v_{A2\boldsymbol{k}\uparrow} \\ v_{A1\boldsymbol{k}\downarrow} & v_{A2\boldsymbol{k}\downarrow} & u_{A1\boldsymbol{k}\downarrow} & u_{A2\boldsymbol{k}\downarrow} \\ u_{B1\boldsymbol{k}\uparrow} & u_{B2\boldsymbol{k}\uparrow} & v_{B1\boldsymbol{k}\uparrow} & v_{B2\boldsymbol{k}\uparrow} \\ v_{B1\boldsymbol{k}\downarrow} & v_{B2\boldsymbol{k}\downarrow} & u_{B1\boldsymbol{k}\downarrow} & u_{B2\boldsymbol{k}\downarrow} \end{pmatrix} \tag{4.14}$$

where the columns are formed by normalised eigenvectors of $\boldsymbol{H_k}$, and the annihilation and creation operators are given by

$$\hat{\Psi}_{\boldsymbol{k}} = U_{\boldsymbol{k}} \hat{A}_{\boldsymbol{k}}, \tag{4.15}$$

where

$$\hat{A}_{\boldsymbol{k}} = \begin{pmatrix} \hat{a}_{1\boldsymbol{k}} \\ \hat{a}_{2\boldsymbol{k}} \\ \hat{a}_{1\boldsymbol{k}}^{\dagger} \\ \hat{a}_{2\boldsymbol{k}}^{\dagger} \end{pmatrix}. \tag{4.16}$$

In conclusion, the SGA Hamiltonian in the homogeneous case is

$$H_{\mathrm{SGA}} = W + \lambda + \sum_{l\boldsymbol{k}} E_{l\boldsymbol{k}} \hat{a}_{l\boldsymbol{k}}^{\dagger} \hat{a}_{l\boldsymbol{k}}, \tag{4.17}$$

where

$$\begin{aligned} W = N \sum_{\sigma f} t_{f\sigma} g_{AB\sigma}^{t} [\chi_{AB\sigma}^{f} + (\chi_{AB\sigma}^{f})^{*}] + N \frac{1}{4} g_{AB}^{J} \sum_{f} J_f [2 m_A m_B \\ + \sum_{\sigma} (2(\Delta_{AB\bar{\sigma}}^{f})^{*} \Delta_{AB\sigma}^{f} - 2(\chi_{AB\bar{\sigma}}^{f})^{*} \chi_{AB\sigma}^{f} - |\chi_{AB\sigma}^{f}|^2 - |\Delta_{AB\sigma}^{f}|^2)], \end{aligned} \tag{4.18}$$

is the sum of Equations (4.3) and (4.5). At this point, the grand potential functional at inverse temperature $\beta = 1/k_{\mathrm{B}}T > 0$ can be evaluated [49] giving

$$\Omega = -\frac{1}{\beta} \ln \mathrm{Tr}(e^{-\beta \hat{H}_{\mathrm{SGA}}}) = W + \lambda - \sum_{l,\boldsymbol{k}} \ln (1 + e^{-\beta E_{l\boldsymbol{k}}}), \tag{4.19}$$

where λ is defined in Equation (4.12).

4.2 Self-Consistent Equations and Equations for Lagrange Multipliers

The expressions for the Lagrange multipliers and self-consistent equations for the mean-fields are obtained by minimising the energy. This is done by taking derivatives with respect to the Lagrange multipliers and mean-fields. Note that the derivatives should be taken separately with respect to the real and imaginary parts. The Lagrange multipliers are given by,

$$\begin{aligned}
\lambda^{\chi^f}_{AB\sigma} =& -t_{f\sigma} g^t_{AB\sigma} + \frac{J_f}{4} g^s_{AB}(2\chi^f_{AB\bar{\sigma}} + \chi^f_{AB\sigma}),\\
\lambda^{\Delta^f}_{AB\sigma} =& -\frac{J_f}{4} g^s_{AB}(2\Delta^f_{AB\bar{\sigma}} - \Delta^f_{AB\sigma}),\\
\lambda^n_{A\sigma} =& -\sum_{\sigma' f} t_{f\sigma'} \frac{\partial g^t_{AB\sigma'}}{\partial dn_{A\sigma}} [\chi^f_{AB\sigma'} + (\chi^f_{AB\sigma'})^*] - \sum_f \frac{J_f g^s_{AB} m_B \Xi_\sigma}{2}\\
& -\sum_f \frac{J_f}{4} \frac{\partial g^J_{AB}}{\partial n_{A\sigma}} [m_A m_B + \sum_{\sigma'} (2(\Delta^f_{AB\bar{\sigma}'})^* \Delta^f_{AB\sigma'} - 2(\chi^f_{AB\bar{\sigma}'})^* \chi^f_{AB\sigma'}\\
& - |\chi^f_{AB\sigma'}|^2 - |\Delta^f_{AB\sigma'}|^2)]
\end{aligned} \tag{4.20}$$

where $\Xi_\uparrow = 1$ and $\Xi_\downarrow = -1$. Note that in the homogeneous case $m_A m_B = -m_A^2$ and thus come with a factor 2 upon derivation. The mean-fields are further calculated using

$$\begin{aligned}
\mathrm{Re}[\chi^f_{AB\sigma}] = -\frac{1}{2}\sum_{l,k} f(E_{lk}) \frac{\partial E_{lk}}{\partial \mathrm{Re}[\lambda^{\chi^f}_{AB\sigma}]},\ \mathrm{Im}[\chi^f_{AB\sigma}] = \frac{1}{2}\sum_{l,k} f(E_{lk}) \frac{\partial E_{lk}}{\partial \mathrm{Im}[\lambda^{\chi^f}_{AB\sigma}]},\\
\mathrm{Re}[\Delta^f_{AB\sigma}] = -\frac{1}{2}\sum_{l,k} f(E_{lk}) \frac{\partial E_{lk}}{\partial \mathrm{Re}[\lambda^{\Delta^f}_{AB\sigma}]},\ \mathrm{Im}[\Delta^f_{AB\sigma}] = \frac{1}{2}\sum_{l,k} f(E_{lk}) \frac{\partial E_{lk}}{\partial \mathrm{Im}[\lambda^{\Delta^f}_{AB\sigma}]},\\
n_{i\sigma} = \frac{1}{2} - \sum_{l,k} f(E_{lk}) \frac{\partial E_{lk}}{\partial \lambda^n_{i\sigma}}.
\end{aligned} \tag{4.21}$$

Where E_{lk} are eigenvalues of the Hamiltonian in Equation (4.10).

4.3 Density of States

Based on the expression of the operators Equation (4.15), the spin dependent density of states (DOS) at energy ω can be calculated by

$$N_{A\sigma}(\omega) = \sum_{l,k} g^N_{A\sigma} [|u_{Alk\sigma}|^2 \delta(\omega - E_{lk}) + |v_{Alk\sigma}|^2 \delta(\omega + E_{lk})]. \tag{4.22}$$

where the δ-functions are approximated by Lorentzians

$$\delta(\omega - E_{nk}) \approx \frac{\Gamma}{\pi} \frac{1}{(\omega - E_{nk})^2 + \Gamma^2} \tag{4.23}$$

with width Γ. See for example [37]. Further, note the Gutzwiller factors that enter into the expression for the DOS. These can be understood as related to hopping in time, probing the DOS by inserting and later removing electrons [24, 25]. Thus it is given by, case II,

$$g^N_{i\sigma} = g^t_{ii\sigma} = \frac{n_i(1-n_i)(1-n_{i\bar{\sigma}})}{(1-n_{i\sigma})(n_i - 2n_{i\uparrow}n_{i\downarrow})}. \tag{4.24}$$

4.4 Results

In the homogenous case it is naturally to present the superconducting mean-field somewhat different to in inhomogeneous space. To do so, the superconducting singlet and triplet mean-fields are expressed

$$\Delta^{Sf}_{AB} = \frac{1}{2}\langle \hat{c}_{A\downarrow}\hat{c}_{B\uparrow} - \hat{c}_{A\uparrow}\hat{c}_{B\downarrow}\rangle = \Delta^f_{AB\uparrow} - \Delta^f_{AB\downarrow},$$
$$\Delta^{Tf}_{AB} = \frac{1}{2}\langle \hat{c}_{A\downarrow}\hat{c}_{B\uparrow} + \hat{c}_{A\uparrow}\hat{c}_{B\downarrow}\rangle = \Delta^f_{AB\uparrow} + \Delta^f_{AB\downarrow},$$

as well as the s- and d-wave components

$$\Delta^s_{AB} = \Delta^{Sx}_{AB} + \Delta^{Sy}_{AB}$$
$$\Delta^d_{AB} = \Delta^{Sx}_{AB} - \Delta^{Sy}_{AB}.$$

In this section the possibility of an s-wave mean-field will be excluded by assumption, therefore the superconducting order is described by its d-wave part Δ^d and triplet part Δ^t, which are the quantities plotted. The same follows for the Lagrange multipliers. Note that the used Hamiltonian and mean-field approximation do not give rise to any triplet pairing of the same spin, that is on form $\hat{c}_{A\sigma}\hat{c}_{A\sigma}$.

Further, it is assumed that the hopping is real and homogeneous in space, $\chi^x_{AB\sigma} = (\chi^x_{AB\sigma})^* = \chi^y_{AB\sigma}$. The same assumptions follow for the Lagrange multipliers. Further, the hopping integral and exchange coupling have been taken to be direction and spin independent $t_{f\sigma} = t$ and $J_f = J$. The hopping integral is taken as unit of energy $t = -1$. The chosen Gutzwiller factors are those referred to as case II in Section 3.1.

Using these assumptions the self-consistent equations in Section 4.2 have been solved for two different exchange couplings J, to facilitate comparisons with the results of the inhomogeneous case in Sections 5.3.1 and 5.4.

4.4.1 Phase Diagrams

The pairing, hopping and antiferromagnetic mean-fields in both the uncorrelated and correlated systems are presented in Figure 4.2. In (a)-(b) for $J = 0.25$ and $J = 1$ in (c)-(d). The x-axis show the entire studied doping region for $J = 1$ which means that the graphs for $J = 0.25$ are cut when the superconductivity approach zero. To better see the coexistence of antiferromagnetism and superconductivity Figure 4.3 focuses on this region. As in Figure 4.2 (a)-(b) show the mean-fields for $J = 0.25$ and (c)-(d) for $J = 1$. In the right column the mean-fields are multiplied by the appropriate Gutzwiller factor.

Without the Gutzwiller factors, all mean-fields increase towards lower dopings, a behaviour similar to results in Refs. [16, 18, 20]. However, in the correlated state, with Guztwiller factors, the hopping and superconducting mean-fields are reduced for lower dopings, the latter reproducing the known dome shape of superconductivity in cuprates [50]. The opposite is true for the antiferromagnetic order, which actually increases in the correlated state.

Further, increasing J shifts the endpoints of the antiferromagnetic and superconducting regions to the right, that is to higher levels of hole doping. Giving larger regions of superconductivity and antiferromagnetisation coexisting with superconductivity. How far into the hole-doped region the antiferromagnetic phase reaches varies between models [18, 20, 25, 43] one reason can be the choice of Gutzwiller factors, see Section 3.1.

It should be pointed out that the Lagrange multipliers are the values entering into the Hamiltonian Equation (4.10) which gouverns the spectrum and the DOS, and not the mean-fields. The Lagrange multipliers connected with the mean-fields in Figure 4.2 are presented in Figure 4.4. In (a)-(b) for $J = 0.25$ and (c)-(d) for $J = 1$, as before the right column shows the entire considered doping region while the right focus on the antiferromagnetic one.

4.4.2 Density of States

The DOS is studied at two different levels of hole doping, $\delta = 0.05$ and $\delta = 0.005$. The higher with $J = 0.25$ and the lower with both $J = 0.25$ and $J = 1$, the latter to allow for comparisons between the antiferromagnetic and non-antiferromagnetic region keeping the same doping. The quantity plotted is always the DOS, given in Equation (4.22), multiplied by Γ. The multiplication is done since the approximation of Dirac delta functions as Lorentzians, see Equation (4.23), gives them height $1/\Gamma$ and $N(\omega)$ dimension 1/energy. The DOS of up spins at sites A is plotted on the y-axis in Figure 4.5, with energy on the x-axis. Since this is the non-antiferromagnetic region, the DOS of down spins looks the same and is therefore not plotted. There is neither any difference between A- and B-sites and the DOS of sites A and B are identical.

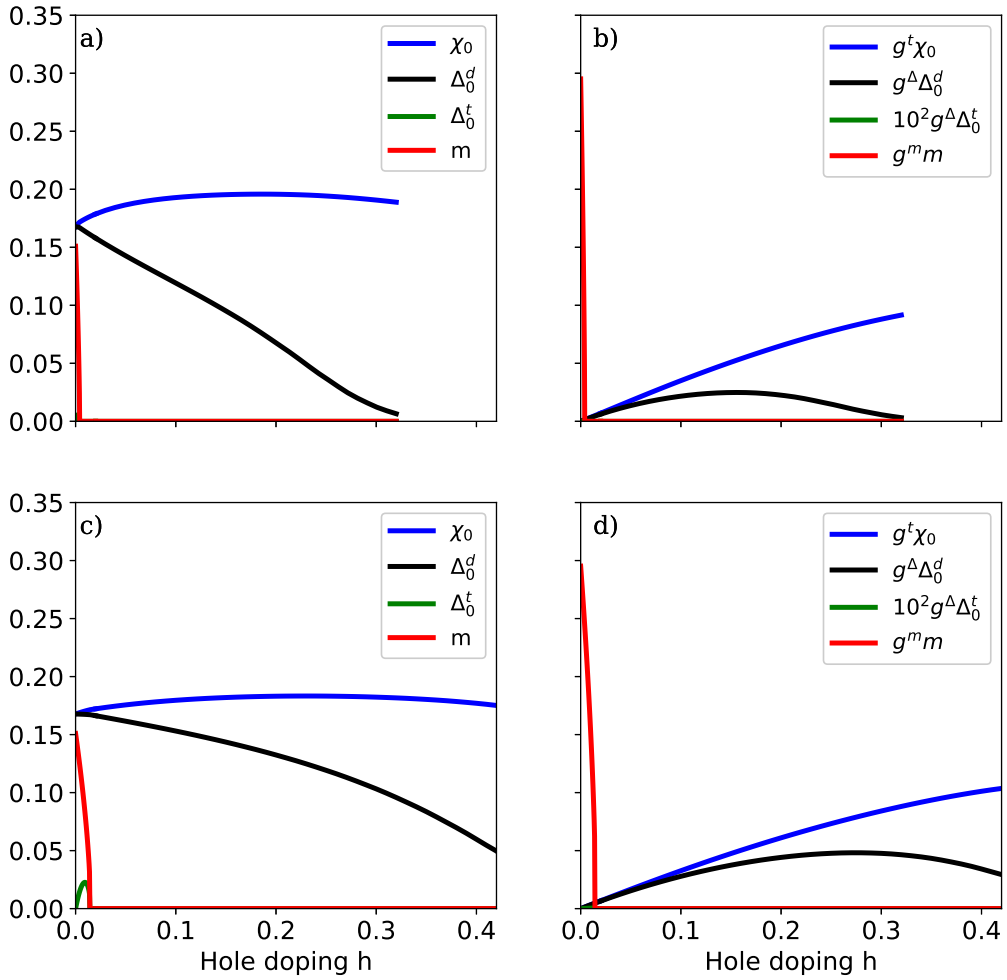

Figure 4.2: *First row, mean-fields for $J = 0.25$ in (a) and multiplied by the appropriate Gutzwiller factor in (b), second row, mean-fields for $J = 1$ in (c) and multiplied by the appropriate Gutzwiller factor in (d), according to legends. The entire considered doping region is plotted, as specified on the x-axes.*

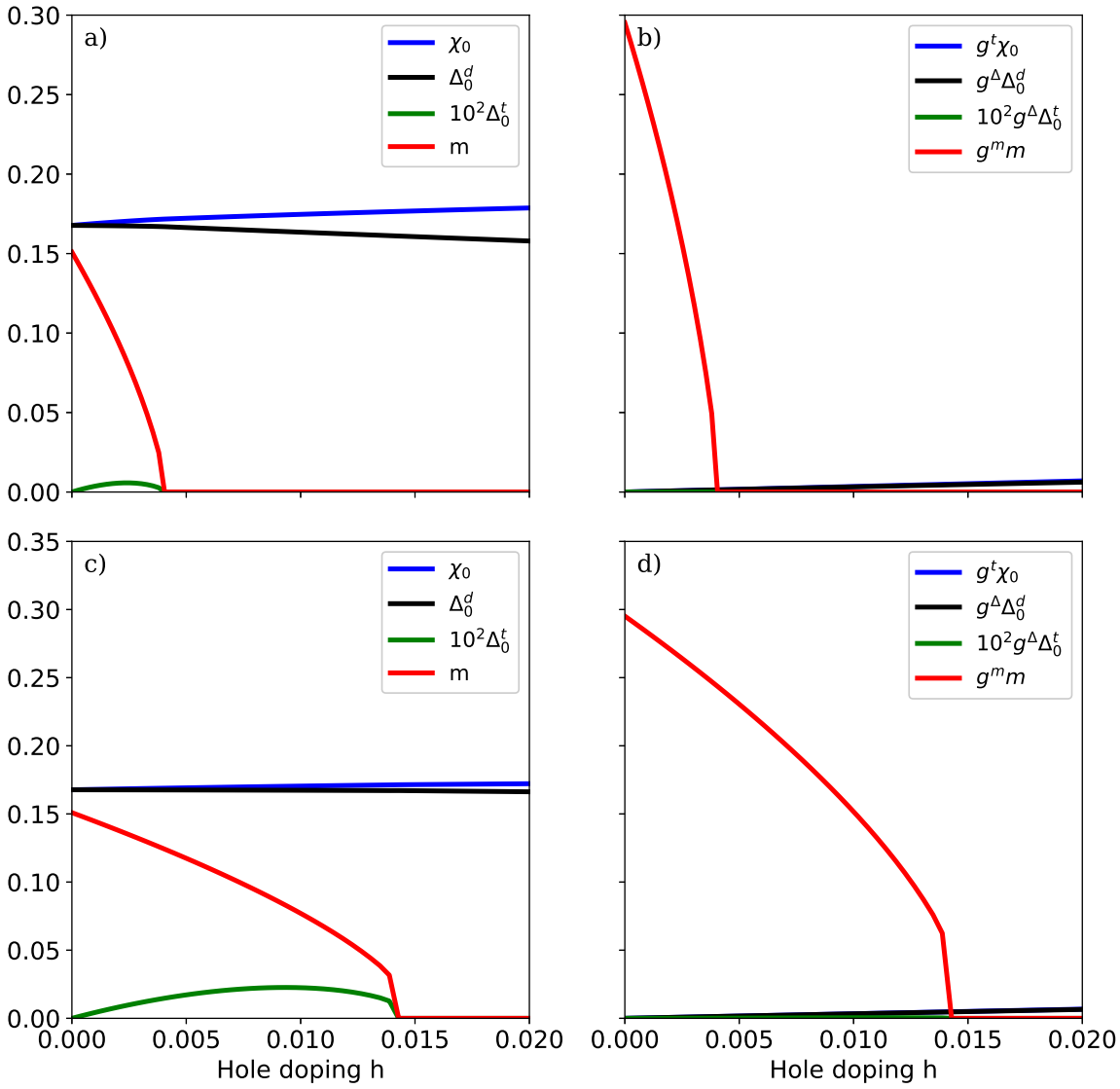

Figure 4.3: *Focus on the region with coexistence of superconductivity and antiferromagnetism. First row, mean-fields for $J = 0.25$ in (a) and multiplied by the appropriate Gutzwiller factor in (b), second row, mean-fields for $J = 1$ in (c) and multiplied by the appropriate Gutzwiller factor in (d), according to legends. Dopings are specified at the x-axes.*

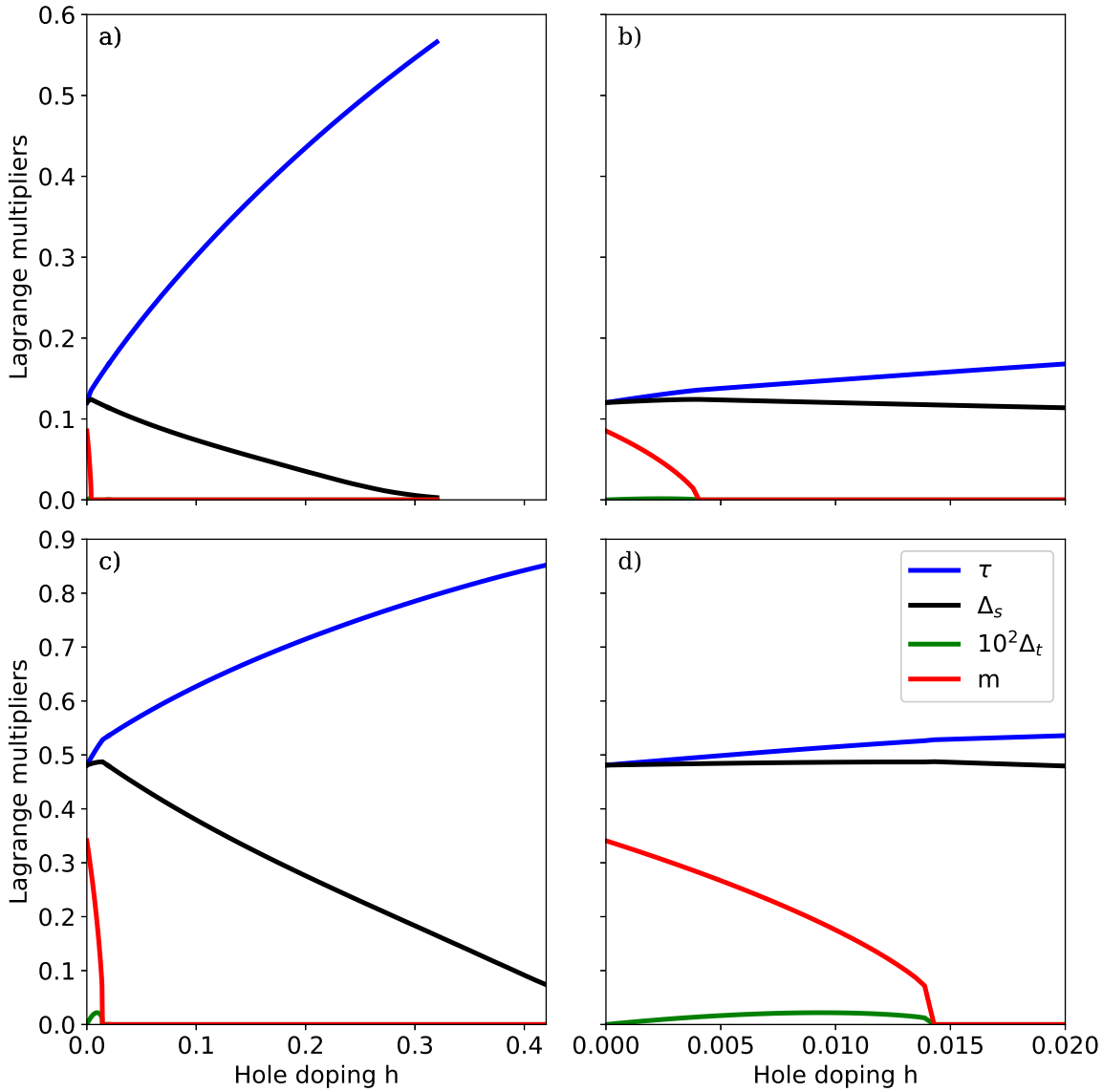

Figure 4.4: *Lagrange multipliers for J=0.25 in (a)-(b) and J=1 in (c)-(d). The left column shows the entire studied doping interval while the right focuses on the region with coexsistence.*

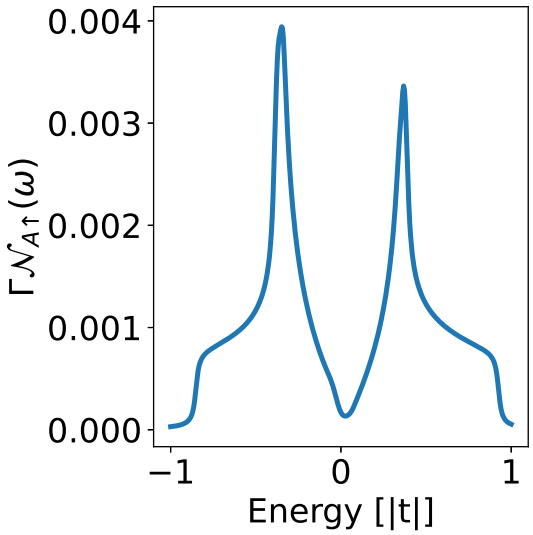

Figure 4.5: *DOS of up spins at sites A at hole doping $\delta = 0.05$ and with $J = 0.25$, at the y-axis, see Equation (4.22), and energy on the x-axis. The system is in the non-antiferromagnetic region and therefore spin down will look the same.*

The lower hole doping $\delta = 0.005$, is first studied for $J = 0.25$ see Figure 4.6(a), where the DOS of up spins is plotted on the y-axis and energy on the x-axis. The system is in the non-antiferromagnetic region, and thus the spin down is equivalent. Increasing the exchange coupling, the system is moved into the antiferromagnetic region and the DOS becomes spin dependent. The DOS for up spins at J=1 can be seen in Figure 4.6(b) and for down spins in Figure 4.6(c) x- and y-axes as in 4.6(a). Since there is a majority spin at sites A the DOS will be spin dependent, so is also the Gutzwiller factor, see Equation (4.24), scaling up and down differently.

As long as there is no net ferromagnetisation it follows that B have the opposite majority spin with the same amplitude. Thus $n_{B\sigma} = n_{A\bar{\sigma}}$ and $m_A = -m_B$. Consequently the DOS will also be site symmetric, $N_{B\bar{\sigma}} = N_{A\sigma}$.

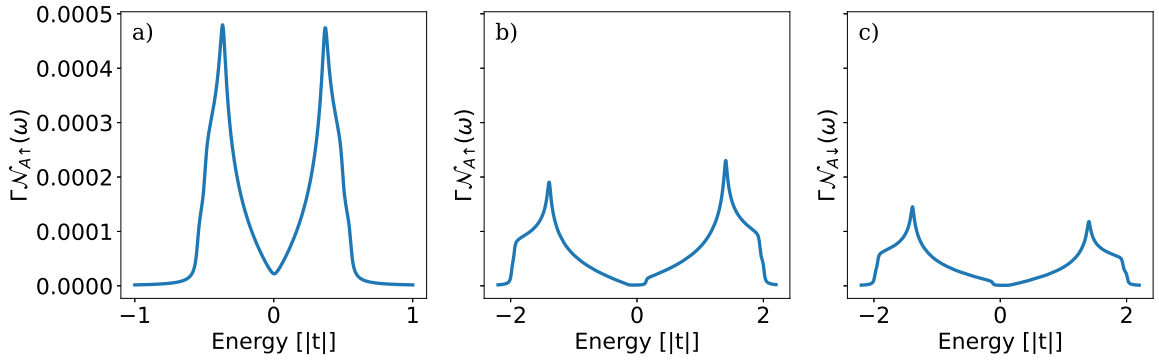

Figure 4.6: *Results for $\delta = 0.005$ in (a) DOS of spin up using J=0.25 (b) DOS of spin up using J=1 and (c) DOS of spin down using J=1. In all, the x-axis gives energy and the DOS, see Equation (4.22), is on the y-axis. In (a) the system is in the non-antiferromagnetic region and therefore spin down will look the same. In (b) and (c) the system is in the region with coexistence so the DOS of both spin up and down are plotted since they are different.*

5 Inhomogenous Case

Now focus is shifted to inhomogeneous systems. Inhomogeneities can be realised in multiple ways, for example by introducing defects or edges. Here, the latter is studied using a slab where the boundaries are cut as [110] edges. At the [110] edges zero-energy Andreev bound states (ABS) arise and mean-fields change compared to in the bulk.

As these systems are not homogeneous and mean-fields vary with distance from the edge, a new unit cell is required and consequently new equations are derived as described in Sections 5.1 and 5.2. The equations are spin dependent and allow for spatially dependent exchange couplings and hopping integrals, the latter is also spin dependent. These equations will be solved at different average hole-dopings

$$1 - \delta = \frac{1}{N_x} \sum_a n_a, \tag{5.1}$$

not to be confused with the local electron density n_a. In the chapter local occupation densities will always be discussed in terms of n_a rather than hole doping $\delta_a = 1 - n_a$, hole doping thus always refer to the global value δ. Further, the Guztwiller factors of Case II in Section 3.1 will be used. In addition, the systems consist of $N_x = 100$ sites, which can be assumed to be the case in the remainder of the chapter. The hopping integral and exchange coupling will be assumed to be uniform and spin independent $t_{ij\sigma} = t$, $J_{ij} = J$ and the hopping χ real. Further, the absolute value of the hopping integral will be taken as the unit of energy $t = -1$.

Using those parameters, results have been generated for $J = 0.25$ getting a superconducting order parameter with pure d-wave symmetry at the edge and at the studied dopings δ. Details of the results can be found in Paper I and are summarised in Section 5.3.1. Increasing the exchange coupling to $J = 0.3$ a subdominant s-wave component of the order parameter was found, see Section 5.3.2. Increasing J even further to $J = 1$ makes it possible to converge the equations at the lower doping $\delta = 0.03$ and thereby study antiferromagnetism (AFM) in slab systems, see Section 5.4. The latter results should provide principle indications of what to expect at sufficiently low average dopings for lower, more realistic, exchange couplings J.

In the chapter, the mean-field Hamiltonian is first evaluated and the self-consistent equations derived. After, results for different exchange couplings J are presented and discussed.

5.1 Evaluation of Mean-Field Hamiltonian

To evaluate the Hamiltonian in Equation (3.38) an appropriate unit cell must be chosen. The unit cell reasonably uses the symmetry of the system and is, for computational reasons, as small as possible. The unit cell (UC) that will be used is shown in Figure 5.1. It is different from the one in the homogenous case, see Figure 4.1, owing to spatial variation along the x'-axis. The unit cell is N_x sites deep, the width of the slab, and the sites are labelled 1,2,...,N_x starting from the right edge. Thus, $N_x/2$ and $N_x/2+1$ are the farthest away from the edge.

Evaluating the Hamiltonian in Equation (3.38), the contribution of the new unit cell to the hopping is

$$\sum_{\substack{UC\\ \sigma}} t_{ij\sigma} g^t_{ij\sigma} \langle \hat{c}^\dagger_{i\sigma} \hat{c}_{j\sigma} + \text{H.C.} \rangle = \sum_{f,\sigma} \sum_{a=1}^{N_x-1} t^f_{a,a+1\sigma} g^t_{a,a+1\sigma} \Big[\chi^f_{a,a+1\sigma} + (\chi^f_{a,a+1\sigma})^* \Big], \tag{5.2}$$

standing at site 1, hopping is possible to site 2 in x- or y-direction. At site 2, hopping is possible to sites 1 and 3, but the former has already been accounted for, etc. The spin term is evaluated as in Section 4 and is given by

$$\begin{aligned} \sum_{\substack{UC\\ \sigma}} J_{ij} g^J_{ij} \langle \boldsymbol{S_i} \cdot \boldsymbol{S_j} \rangle = \frac{1}{4} \sum_f \sum_{a=1}^{N_x-1} J^f_{a,a+1} g^J_{a,a+1} \Big[2 m_a m_{a+1} + \sum_\sigma \Big(2 \Delta^{f*}_{a,a+1\bar{\sigma}} \Delta^f_{a,a+1\sigma} \\ - 2 \chi^{f*}_{a,a+1\bar{\sigma}} \chi^f_{a,a+1\sigma} - |\Delta^f_{a,a+1\sigma}|^2 - |\chi^f_{a,a+1\sigma}|^2 \Big) \Big], \end{aligned} \tag{5.3}$$

where $f \in \{x, y\}$. The expectation value of the energy per unit cell is then

$$\begin{aligned} W_{110} = \sum_f \sum_{a=1}^{N_x-1} \Bigg\{ \sum_\sigma t^f_{a,a+1\sigma} g^t_{a,a+1\sigma} \Big[\chi^f_{a,a+1\sigma} + (\chi^f_{a,a+1\sigma})^* \Big] \\ + \frac{J^f_{a,a+1}}{4} g^J_{a,a+1} \Big[2 m_a m_{a+1} + \sum_\sigma \Big(2 \Delta^{f*}_{a,a+1\bar{\sigma}} \Delta^f_{a,a+1\sigma} \\ - 2 \chi^{f*}_{a,a+1\bar{\sigma}} \chi^f_{a,a+1\sigma} - |\Delta^f_{a,a+1\sigma}|^2 - |\chi^f_{a,a+1\sigma}|^2 \Big) \Big] \Bigg\}. \end{aligned} \tag{5.4}$$

The same calculations for the scalar terms of mean-fields times Lagrange multipliers give per unit cell

$$\begin{aligned} \tilde{\lambda}_{110} = \sum_{f,\sigma} \sum_{a=1}^{N_x-1} \Big[\chi^f_{a,a+1\sigma} \lambda^{\chi^f}_{a,a+1\sigma} + (\chi^f_{a,a+1\sigma} \lambda^{\chi^f}_{a,a+1\sigma})^* + \\ \Delta^f_{a,a+1\sigma} \lambda^{\Delta^f}_{a,a+1\sigma} + (\Delta^f_{a,a+1\sigma} \lambda^{\Delta^f}_{a,a+1\sigma})^* \Big] + \sum_\sigma \sum_{a=1}^{N_x} \lambda^n_{a\sigma} n_{a\sigma} \end{aligned} \tag{5.5}$$

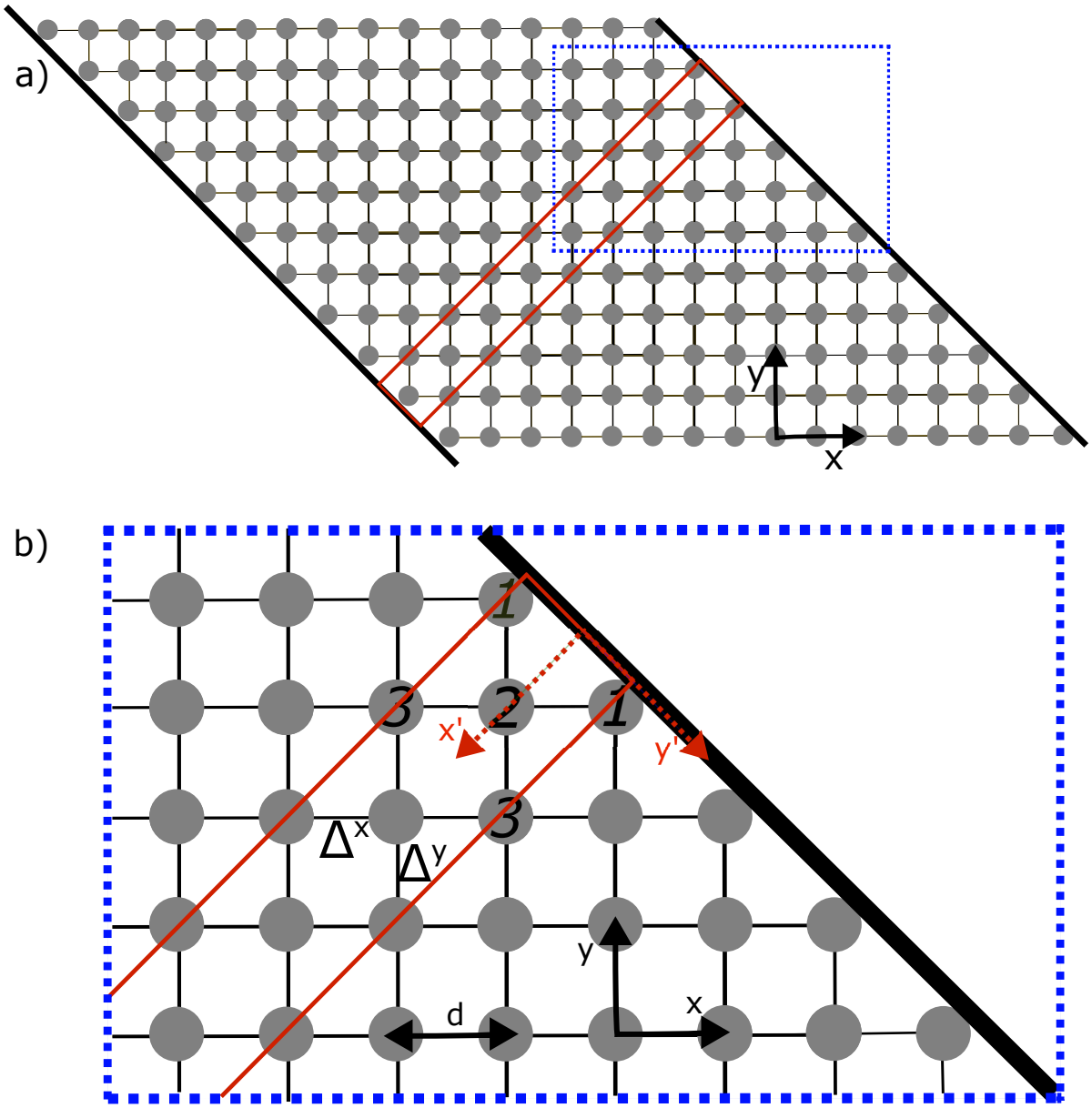

Figure 5.1: *(a) The studied slab with sites, as grey disks, arranged into a square lattice with lattice constant d. The edges are cut in the* [110]*-direction. Red lines mark the unit cell and translational invariance along the edge tangent is assumed. The x- and y-axes are the crystal axes, corresponding to the x- and y-axes in Figure 1.2. Between sites the lines represents links which can be in either x- or y-direction. In (b) enlarged view of the area surrounded by dotted blue lines in (a), including the right* [110] *edge. The symmetry axes x' and y' of the unit cell are marked. The axes are chosen so that y' is aligned with the edge tangent and x' with the edge normal. The sites in the unit cell are labelled $a = 1, 2, 3$, etc. after their distance to the right edge measured along x'. Note that it is important to differentiate between the pairing amplitudes $\Delta^x_{a,a+1}$ and $\Delta^y_{a,a+1}$ if both d-wave and extended s-wave symmetries should be considered. There is one link in the y-direction and one in the x-direction between each pair of sites a and $a+1$. Same Figure as Figure 1 in Paper I.*

As the lattice is only translationally invariant along the y'-axis, the Fourier transformation is done in only one dimension according to

$$\begin{aligned}\hat{c}_{ab\sigma} &= \frac{1}{\sqrt{N_y}} \sum_k \hat{c}_{ak\sigma} e^{ikb}, \\ \hat{c}^\dagger_{ab\sigma} &= \frac{1}{\sqrt{N_y}} \sum_k \hat{c}^\dagger_{ak\sigma} e^{-ikb},\end{aligned} \tag{5.6}$$

where the site index i is expressed by its coordinates a and b along the x'- and y'-axes respectively and N_y are the number of sites in the y-direction. So $i \to ab$, and $k \in (-1/(d\sqrt{2}), 1/(d\sqrt{2})]$. For each site, a vector of operators

$$\hat{\psi}_{ak} = \begin{pmatrix} \hat{c}_{ak\uparrow} \\ \hat{c}^\dagger_{a-k\downarrow} \end{pmatrix} \tag{5.7}$$

is introduced. These vectors form the full vector

$$\hat{\Psi}^\dagger_k = (\hat{\psi}^\dagger_{1k}, \hat{\psi}^\dagger_{2k}, \ldots, \hat{\psi}^\dagger_{N_x k}). \tag{5.8}$$

Using the full vector, the operator part can be written as

$$\sum_k \hat{\Psi}^\dagger_k \boldsymbol{H}_k \hat{\Psi}_k, \tag{5.9}$$

where the Hamiltonian matrix $\boldsymbol{H}_k$ consists of blocks on the diagonal, coupling neighbouring sites a and $a+1$,

$$(\boldsymbol{H}_k)_{a,a+1} = \begin{pmatrix} -\lambda^n_{a\uparrow} - \mu & 0 & -2\lambda^\chi_{a,a+1\uparrow} \cos\frac{kd}{\sqrt{2}} & \eta^-_{a,a+1\uparrow}(k)^* \\ 0 & \lambda^n_{a\downarrow} + \mu & -\eta^+_{a,a+1\downarrow}(k) & 2\lambda^{\chi*}_{a,a+1\downarrow} \cos\frac{kd}{\sqrt{2}} \\ -2\lambda^{\chi*}_{a,a+1\uparrow} \cos\frac{kd}{\sqrt{2}} & -\eta^+_{a,a+1\downarrow}(k)^* & -\lambda^n_{a+1\uparrow} - \mu & 0 \\ \eta^-_{a,a+1\uparrow}(k) & 2\lambda^\chi_{a,a+1\downarrow} \cos\frac{kd}{\sqrt{2}} & 0 & \lambda^n_{a+1\downarrow} + \mu \end{pmatrix}, \tag{5.10}$$

where

$$\eta^\pm_{aa'\sigma}(k) = \lambda^{\Delta^x}_{aa'\sigma} e^{\pm\frac{ikd}{\sqrt{2}}} + \lambda^{\Delta^y}_{aa'\sigma} e^{\mp\frac{ikd}{\sqrt{2}}}. \tag{5.11}$$

The commutation of $\hat{c}^\dagger_{-\boldsymbol{k}\downarrow} \hat{c}_{-\boldsymbol{k}\downarrow}$ gives as in the homogenous case, Section 4, an extra term $-\sum_{a=1}^{N_x} (\lambda_{a\downarrow} + \mu)$, so

$$\lambda_{110} = \tilde{\lambda}_{110} - \sum_{a=1}^{N_x} (\lambda_{a\downarrow} + \mu), \tag{5.12}$$

is defined.

To arrive at a scalar expression of the grand potential functional Equation (3.39) the Hamiltonian $\boldsymbol{H}_k$ needs to be diagonalised. As in Section 4.2 a Bougliobov transformation may be applied writing the Hamiltonian

$$\boldsymbol{H}_k = U_k D_k U^\dagger_k, \tag{5.13}$$

where D_k is diagonal with the eigenvalues E_{lk} on the diagonal, and

$$U_k = \begin{pmatrix} u_{11k\uparrow} & ... & u_{1Nk\uparrow} & v_{11k\uparrow} & ... & v_{1Nk\uparrow} \\ v_{21-k\downarrow} & ... & v_{2N-k\downarrow} & u_{21-k\downarrow} & ... & u_{2Nk\downarrow} \\ ... & ... & ... & ... & ... & ... \\ ... & ... & ... & ... & ... & ... \\ u_{N1k\uparrow} & ... & u_{NNk\uparrow} & v_{N1k\uparrow} & ... & v_{NNk\uparrow} \\ v_{N1-k\downarrow} & ... & v_{NN-k\downarrow} & u_{N1-k\downarrow} & ... & u_{NNk\downarrow} \end{pmatrix}, \tag{5.14}$$

where the columns are made up of eiegenvectors of $\boldsymbol{H}_k$. The operators are also transformed using U_k as

$$\hat{\Psi}_k = U_k \hat{A}_k, \tag{5.15}$$

where

$$\hat{A}_k = \begin{pmatrix} a_1 \\ ... \\ a_N \\ a_1^\dagger \\ ... \\ a_N^\dagger \end{pmatrix} \tag{5.16}$$

and E_{1k} is the most negative eigenvalue, E_{2k} the second most negative, and so on.

In conclusion, the SGA Hamiltonian is for the slab system

$$H_{\mathrm{SGA}}^{[110]} = N_y W_{110} + N_y \lambda_{110} + \sum_{l,k} E_{lk} \hat{a}_{lk}^\dagger \hat{a}_{lk} \tag{5.17}$$

and the grand potential functional at inverse temperature $\beta = 1/k_{\mathrm{B}}T > 0$ becomes after diagonalisation

$$\Omega = -\frac{1}{\beta} \ln \mathrm{Tr}(e^{-\beta \hat{H}_{\mathrm{SGA}}^{110}}) = N_y W_{110} + N_y \lambda_{110} - \sum_{l,k} \ln\left(1 + e^{-\beta E_{lk}}\right), \tag{5.18}$$

where N_y is the number of sites in the y-direction and W_{110}, and λ_{110} are defined in Equations (5.4), and (5.12).

5.2 Self-Consistent Equations and Equations for Lagrange Multipliers

The site dependent Lagrange multipliers and self-consistent equations for the mean-fields are obtained by minimising the grand potential functional with respect to the mean-fields and Lagrange multipliers respectively. Note that for values which may be complex, the derivatives of the real and imaginary parts should be considered separately. The Lagrange multipliers are given by

$$\lambda_{a,a+1\sigma}^{\chi^f} = -t_{a,a+1\sigma}^f g_{a,a+1\sigma}^t + g_{a,a+1}^J \frac{J_{a,a+1}^f}{4} \left[2\chi_{a,a+1\bar{\sigma}}^f + (\chi_{a,a+1\sigma}^f)^* \right], \tag{5.19}$$

$$\lambda^{\Delta^f}_{a,a+1\sigma} = -g^J_{a,a+1}\frac{J^f_{a,a+1}}{4}\Big[2(\Delta^f_{a,a+1\bar{\sigma}})^* - (\Delta^f_{a,a+1\sigma})^*\Big], \tag{5.20}$$

$$\lambda^n_{a\sigma'} = \mathcal{T}_{a\sigma'} + \mathcal{M}_{a\sigma'} + \mathcal{J}_{a\sigma'}, \tag{5.21}$$

where

$$\begin{aligned}\mathcal{T}_{a\sigma'} = -\sum_{f,\sigma}\Bigg\{ & t^f_{a,a+1\sigma}\frac{\partial g^t_{a,a+1\sigma}}{\partial n_{a\sigma'}}\Big[\chi^f_{a,a+1\sigma} + (\chi^f_{a,a+1\sigma})^*\Big] \\ & + t^f_{a-1,a\sigma}\frac{\partial g^t_{a-1,a\sigma}}{\partial n_{a\sigma'}}\Big[\chi^f_{a-1,a\sigma} + (\chi^f_{a-1,a\sigma})^*\Big]\Bigg\},\end{aligned} \tag{5.22}$$

$$\begin{aligned}\mathcal{M}_{a\sigma'} = -\frac{J^f_{a,a+1}}{2}\Bigg(& g^J_{a,a+1}\Xi_{\sigma'}m_{a+1} + \frac{\partial g^J_{a,a+1}}{\partial n_{a\sigma'}}m_a m_{a+1} \\ & + g^J_{a-1,a}\Xi_{\sigma'}m_{a-1} + \frac{\partial g^J_{a-1,a}}{\partial n_{a\sigma'}}m_{a-1}m_a\Bigg),\end{aligned} \tag{5.23}$$

where $\Xi_\uparrow = 1$ and $\Xi_\downarrow = -1$, and

$$\begin{aligned}\mathcal{J}_{a\sigma'} = -\frac{1}{4}\sum_{f,\sigma}\Bigg\{ & J^f_{a,a+1}\frac{\partial g^J_{a,a+1}}{\partial n_{a\sigma'}}\Big[2(\Delta^f_{a,a+1\sigma})^*\Delta^f_{a,a+1\bar{\sigma}} - |\Delta^f_{a,a+1\sigma}|^2 \\ & - 2\chi^f_{a,a+1\sigma}\chi^f_{a,a+1\bar{\sigma}} - |\chi^f_{a,a+1\sigma}|^2\Big] + J^f_{a-1,a}\frac{\partial g^J_{a-1,a}}{\partial n_{a\sigma'}} \\ & \Big[2(\Delta^f_{a-1,a\sigma})^*\Delta^f_{a-1,a\bar{\sigma}} - |\Delta^f_{a-1,a\sigma}|^2 - 2\chi^f_{a-1,a\sigma}\chi^f_{a-1,a\bar{\sigma}} - |\chi^f_{a-1,a\sigma}|^2\Big]\Bigg\}.\end{aligned} \tag{5.24}$$

The self-consistent equations read

$$\mathrm{Re}[\chi^f_{a,a+1\sigma}] = -\frac{1}{2N_y}\sum_{l,k} f(E_{lk})\frac{\partial E_{lk}}{\partial \mathrm{Re}[\lambda^{\chi^f}_{a,a+1\sigma}]}, \tag{5.25}$$

$$\mathrm{Im}[\chi^f_{a,a+1\sigma}] = \frac{1}{2N_y}\sum_{l,k} f(E_{lk})\frac{\partial E_{lk}}{\partial \mathrm{Im}[\lambda^{\chi^f}_{a,a+1\sigma}]}, \tag{5.26}$$

$$\mathrm{Re}[\Delta^f_{a,a+1\sigma}] = -\frac{1}{2N_y}\sum_{l,k} f(E_{lk})\frac{\partial E_{lk}}{\partial \mathrm{Re}[\lambda^{\Delta^f}_{a,a+1\sigma}]}, \tag{5.27}$$

$$\mathrm{Im}[\Delta^f_{a,a+1\sigma}] = \frac{1}{2N_y}\sum_{l,k} f(E_{lk})\frac{\partial E_{lk}}{\partial \mathrm{Im}[\lambda^{\Delta^f}_{a,a+1\sigma}]}, \tag{5.28}$$

and

$$n_{i\sigma} = \delta_{\sigma,\downarrow} - \frac{1}{N_y}\sum_{l,k} f(E_{lk})\frac{\partial E_{lk}}{\partial \lambda^n_{i\sigma}}. \tag{5.29}$$

Where E_{lk} are the eigenvalues of $\boldsymbol{H}_k$.

The local density of states (LDOS) is given by

$$N_{i\sigma}(\omega) = \sum_{n,k} g_{i\sigma}^{N} \Big\{ |U_k[2i-1,n]|^2 \delta(\omega - E_{nk}) + |U_k[2i-1,n+N]|^2 \delta(\omega + E_{nk}) \Big\}, \quad (5.30)$$

where the δ-functions are approximated as Lorentzians, see Equation (4.23), and the Gutzwiller factor $g_{i\sigma}^{N}$ is as in Equation (4.24).

5.3 Superconductivity Without Antiferromagnetism

All results presented in the section and in the rest of the chapter are generated assuming a real hopping $\chi_{ij\sigma} = \chi_{ij\sigma}^{*}$ and the same for the corresponding Lagrange multiplier. Further, the hopping integral and exchange coupling are assumed to be site, direction, and spin independent $J_{a,a+1}^{f} = J$ and $t_{a,a+1\sigma}^{f} = t$. The value of $t = -1$ sets the magnitude of the energy scale. In this section the studied average hole doping range is $\delta \in [0.05, 0.2]$

As can be seen in Figure 4.3 antiferromagnetism is arising in the systems at rather low hole doping. By keeping away from that region, the system is in a non-antiferromagnetic phase, effectively making the system independent of spin. Parts of the non-antiferromagnetic region for the slab system with [110] edges was studied in Paper I. Adding the novelty, compared to previous works [36], of allowing the electrons to redistribute in the sample. In this section Paper I with results using $J = 025$ is shortly summarised and results for higher $J = 0.33$ where an s-wave occur discussed.

5.3.1 Summary of Paper I - $J = 0.25$

In Paper I it was found that the edge attracts charges and the local occupation increases, decreasing the local hole doping. The increased occupation reduces the hopping Gutzwiller factor g^t, see Equation (3.16), locally - a sign of increased correlation. It can be understood as when more sites are occupied, the electrons are less free to move. The redistribution of charges causes the d-wave pairing mean-field to be less suppressed at the edge and that there is no room for an s-wave part to arise as a difference to uniform electron density $n_a = 1 - \delta$ as in [36].

It is important to note that the mean-fields are computed in the uncorrelated state. Considering the correlated state, the mean-fields are multiplied by the appropriate Guztwiller factor. As the Gutzwiller factor is decreased at the edge, this actually means the superconducting order parameter is reduced at the edge even when the superconducting mean-field is not.

It should be noted that no AFM was found in Paper I, why expressions and derivations in the paper are spin independent. Meaning, for example $n_{i\uparrow} = n_{i\downarrow}$

and $g^{\Delta}_{ij\sigma} = g^{t}_{ij}$. However, the results were obtained using the equations in Section 5.2.

5.3.2 Higher Exchange Coupling - $J = 0.33$

As discussed in Section 4.4 the phase diagram is dependent on the exchange coupling J. Adjusting J it is also possible to change the symmetry of the order parameter. When increasing J to 0.33, keeping all other parameters, a combined $d + is$ symmetry at the edge for has been found, see Figure 5.2. In Figure 5.2 the local occupation and hopping are plotted in (a) and (b), the d-wave and s-wave combinations of the pairing amplitudes in (c) and (d) respectively and the corresponding expressions for the superconducting order parameter in (e) and (f). In all cases with the site or link number on the x-axis measured from the edge. There is no qualitative difference in the occupation profile compared to when $J = 0.25$. The edge attracts electrons and the d-wave superconducting mean-field and order parameter are suppressed close to the edge. The hopping is also qualitatively behaving as for $J = 0.25$. The difference lies in there being an s-wave in both the uncorrelated and correlated state. This is consistent with Reference [34] where a subdominant s-wave was found in a two-dimensional system using the Gutzwiller approximation.

The presence of the subdominant s-wave means a uniform gap opens at the edge. The gap results in the Andreev bound states being moved away from zero energy and the Andreev peak splits. The effect can be seen in Figure 5.3(b) where the LDOS in the gap is plotted with energy on the y-axis, site number on the x-axis and values indicated by the colourbar. In Figure 5.3(a) the entire LDOS is plotted. Note that in contrast to the case of $\delta = 0.05$, see Paper I, there is some weight of ABS on even sites. But it is still considerably lower than on odd sites. That is also the case for $\delta = 0.2$ and $J = 0.25$. The increased localisation of ABS to every second site, when doping is reduced, may thus be an effect of the increased correlation.

5.4 Coexistence of Antiferromagnetism and d-Wave Superconductivity - $J = 1$

The inhomogeneous case has also been studied for lower dopings. As the occupation is still increasing and approaching 1, converging these systems are challenging. By using $J = 1$ it is possible to reach antiferromagnetic (AFM) order already at higher average hole dopings, see Figure 4.3. Doing so AFM, have been found already at $\delta = 0.03$, higher than in the homogenous case, where it is present from approximately $\delta = 0.014$, see Figure 4.3(c)-(d). Results were generated with the same assumptions as specified in Section 5.3 with the addition of the d-wave

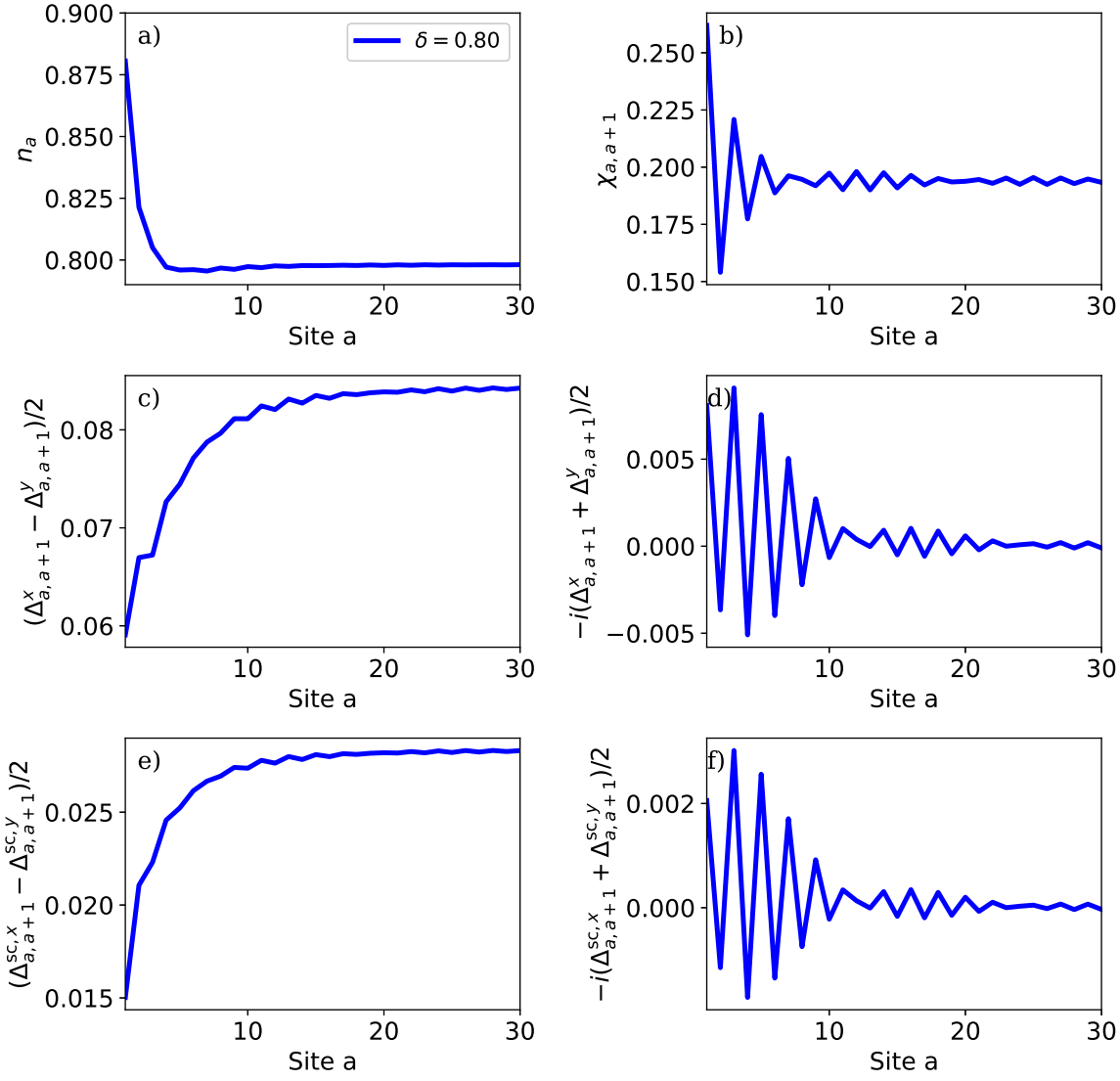

Figure 5.2: *(a) Spatially dependent electron densities n_a, (b) hopping amplitude $\chi_{a,a+1}$, (c) combination of pairing amplitudes corresponding to d-wave character $(\Delta^x_{a,a+1} - \Delta^y_{a,a+1})/2$, (d) combination of pairing amplitudes corresponding to s-wave character $(\Delta^x_{a,a+1} + \Delta^y_{a,a+1})/2$ multiplied by the negative imaginary unit $-i$, (c) combination of superconducting order parameters corresponding to d-wave character $(\Delta^{\mathrm{SC,x}}_{a,a+1} - \Delta^{\mathrm{SC,y}}_{a,a+1})/2$ and (f) combination of superconducting order parameters corresponding to s-wave character $(\Delta^{\mathrm{SC,x}}_{a,a+1} + \Delta^{\mathrm{SC,y}}_{a,a+1})/2$ once more multiplied by $-i$. All quantities are for $\delta = 0.80$ given in the legend. The slab width is $N_x = 100$, but only the first $a \in [1, 30]$ sites/links are shown.*

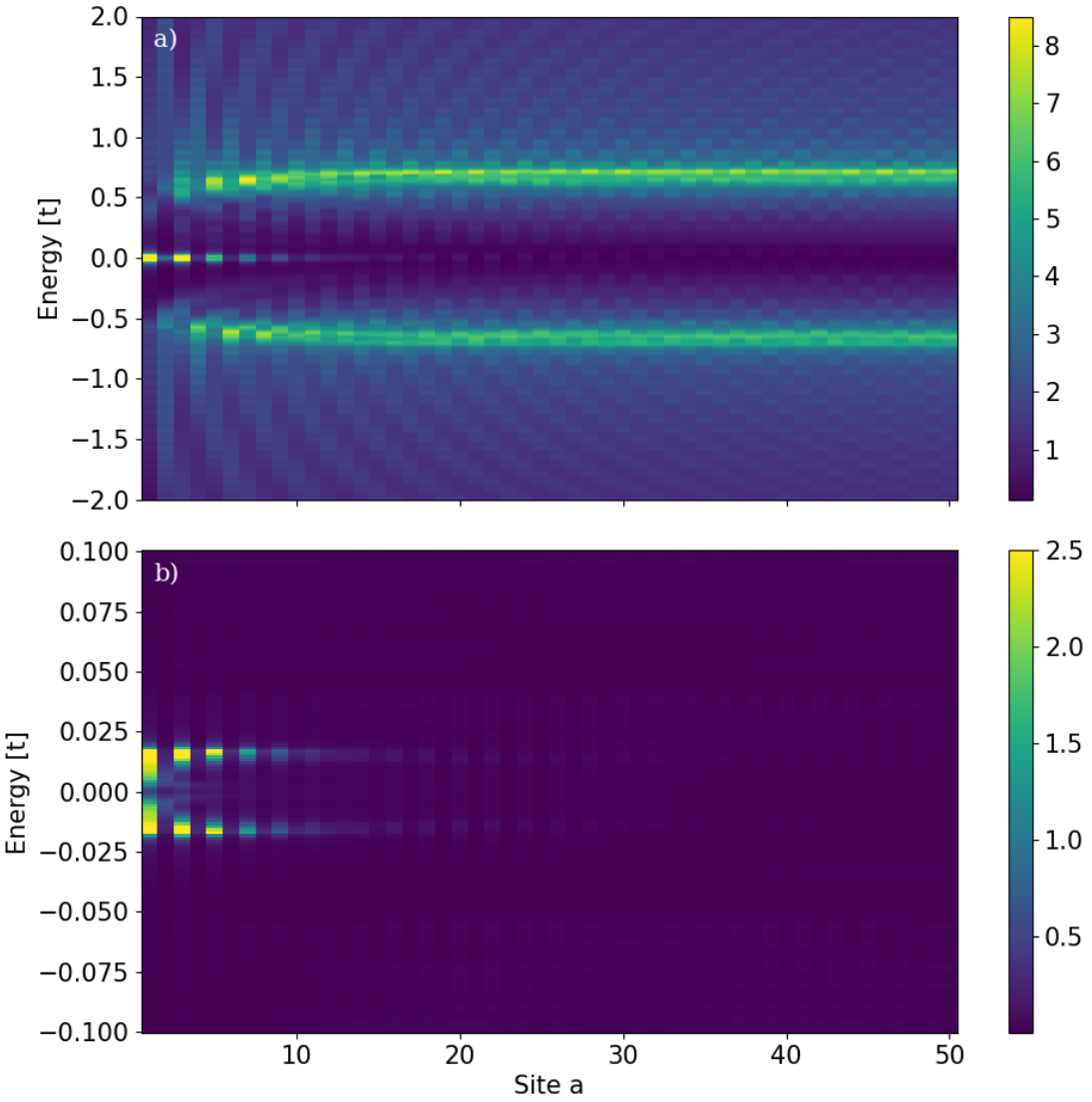

Figure 5.3: *Local density of states* $\Gamma\mathcal{N}_a(\omega)$ *for* $N_x = 100$, $\delta = 0.8$ *and* $J = 0.3$. *In (a) the full spectrum as function of coordinate a is shown using* $\Gamma = 0.015$. *(b) Focus on the low-energy part of the spectrum, where the zero-energy Andreev bound states are clearly seen as well as the split of them due to the s-wave component, generated with a smaller* $\Gamma = 0.001$.

component being forced to be real and s-wave imaginary. With a converged solution the constraint have been relaxed at the converged solution found to be stable. In the section will first the calculated mean-fields be discussed and then the associated LDOS.

5.4.1 Mean-Fields

In Figure 5.4 mean-fields and Guztwiller factors of the inhomogenous case in the antiferromagnetic region, with J=1 and $\delta = 0.03$, is shown. As for the non-antiferromagnetic case electrons are attracted to the edge see Figure 5.4(a) where the occupation as function of site is shown. The relative difference in local occupation is smaller than, for example $\delta = 0.8$ see Figure 2 in Paper I, probably since n=1 constitutes an upper limit and therefore limits the possible range of occupations. In (b) the antiferromagnetisation, $m_a = n_{a\uparrow} - n_{a\downarrow}$ is plotted. Closer to the edge m has a magnitude and changes sign in between sites, indicating antiferromagnetism, towards the middle the amplitude decreases though some oscillations remain. It remains to conclude whether the antiferromagnetisation is simply a result of the higher edge occupation, putting the region locally in the antiferromagentic region see again Figure 4.3, or some more intricate edge physics.

Further, Figures 5.4 c) and d) show the singlet, $\Delta_{a,a+1,\uparrow} - \Delta_{a,a+1,\downarrow}$, and triplet, $\Delta_{a,a+1,\uparrow} + \Delta_{a,a+1,\downarrow}$, combinations of the superconducting mean-fields. Note that due to the presence of antiferromagnetisation there is also a triplet superconducting mean-field close to the edge, which dies towards the middle of the slab. Also note that the singlet has a pure d-wave symmetry. In (e) and (f) the corresponding superconducting order parameters are shown, calculated by multiplying by the appropriate Gutzwiller factor, as $\Delta_{a,a+1,\uparrow} g^{\Delta}_{a,a+1\uparrow} - \Delta_{a,a+1,\downarrow} g^{\Delta}_{a,a+1\downarrow}$, $\Delta_{a,a+1,\uparrow} g^{\Delta}_{a,a+1\uparrow} + \Delta_{a,a+1,\downarrow} g^{\Delta}_{a,a+1\downarrow}$. The singlet superconductivity is, as in the non-antiferromagnetic region, decreased by the Gutzwiller factors, especially so close to the edge where it is almost vanishing. Interestingly, that is not the case for triplet superconductivity, which amplitude is actually increased and shifted into becoming more symmetric around zero. Mathematically, this is the result of the Guztwiller factors being spin dependent and therefore changing the relation between $\Delta_{a,a+1,\uparrow}$ and $\Delta_{a,a+1,\downarrow}$. Since the Gutzwiller factor for magnetism, see Equation 3.21, is larger than 1 the magnetism is strengthened. As the triplet superconductivity is related to the AFM, it is perhaps not surprising that the Gutzwiller factors also increase the triplet superconducting order parameter.

For completeness the hopping is plotted in Figure 5.4(g) and the Gutzwiller factors for hopping and superconductivity in (h). Towards the middle as the system tends to be spin-independent the Gutzwiller factors are the same. While closer to the edge especially $g^{\Delta}_{a,a+1\sigma}$ depends on spin and oscillates, the cause of the strengthening of the triplet superconductivity. The tendency towards AFM $n_{a\sigma} \approx n_{a+1\bar{\sigma}}$ strives to reduce the spin dependence of the Gutzwiller factor for

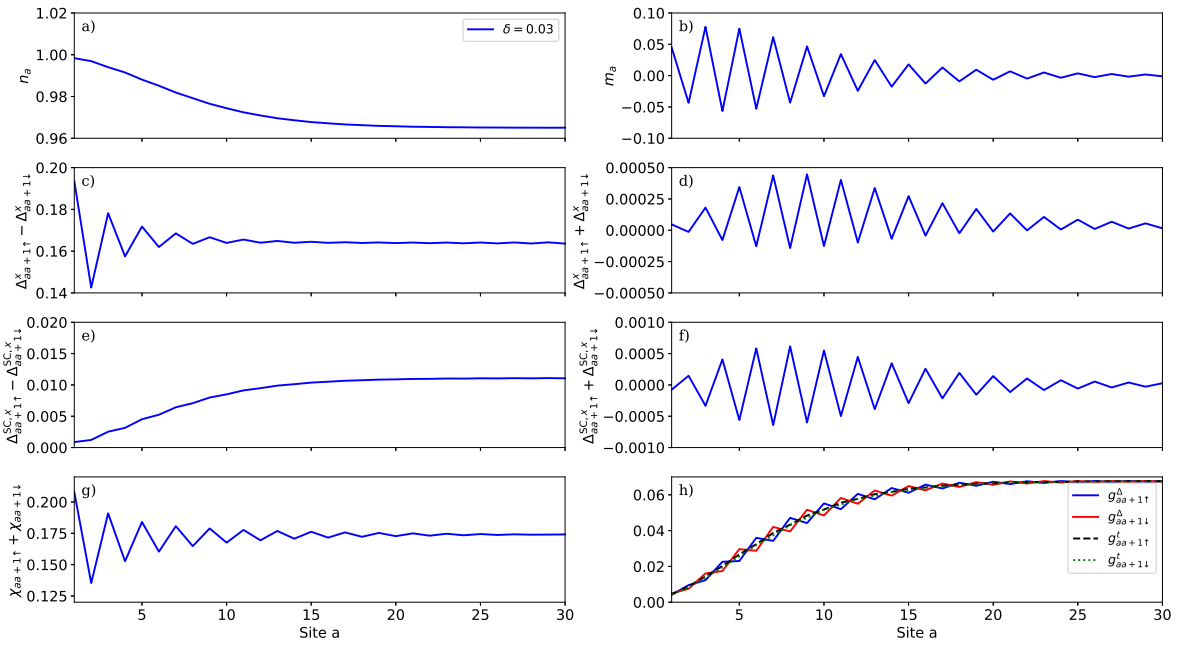

Figure 5.4: *Results for average hole doping $\delta = 0.03$ using J=1. In (a) the occupation is plotted and in (b) the magnetisation. The singlet superconductivity, $\Delta^x_{a,a+1,\uparrow} - \Delta^x_{a,a+1,\downarrow}$, in (c) and the triplet, $\Delta^x_{a,a+1,\uparrow} + \Delta^x_{a,a+1,\downarrow}$, in (d). In (e) and (f) the superconducting order parameter is shown, singlet, $\Delta^{\mathrm{SC},x}_{a,a+1,\uparrow} - \Delta^{\mathrm{SC},x}_{a,a+1,\uparrow}$ and triplet, $\Delta^{\mathrm{SC},x}_{a,a+1,\uparrow} + \Delta^{\mathrm{SC},x}_{a,a+1,\uparrow}$, respectively. In (g) the hopping mean-field is plotted. In (a)-(g) the legend in (a) indicates the occupations. In (h) the spin dependent Gutzwiller factors for hopping and superconductivity are plotted as stated by the legend. All plots are having site number on the x-axis.*

hopping g^t.

5.4.2 Density of States

The LDOS for the entire spectrum is shown in Figure 5.5(a) and for the low energy region in Figure 5.5(b). Site on the x-axis and energy on the y-axis. The peaks due to the Andreev zero-energy states can be seen as well as the spin-split of them because of the AFM. Cuts of the same DOS are presented in Figure 5.6, the entire spectrum in the left colon and the low energy part in the right. Sites and spins are indicated by the legends. The spin splitting is seen in (a)-(d) and the splitting of the ABS in (f) and (h)-(j). Especially in (j) there is almost no overlap of the peaks. Due to the combination of the Gutzwiller factors being site-dependent and the ABS only living at odd sites, the ABS of spins up constantly have higher weight than the ABS of spins down.

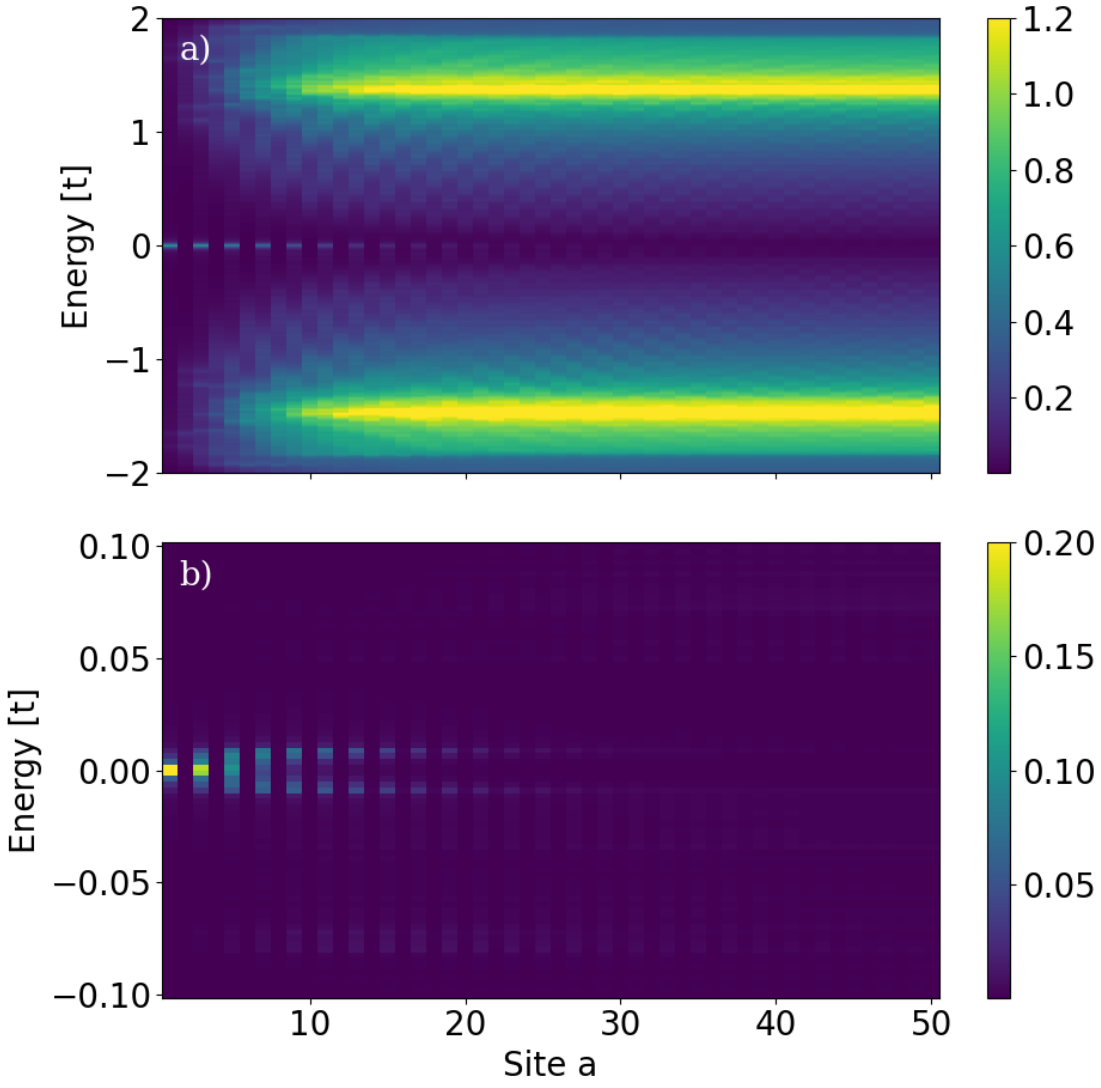

Figure 5.5: *The full DOS in (a) as a function of coordinate a generated using* $\Gamma = 0.015$*,* $J = 1$ *and* $\delta = 0.03$*. (b) Focuses on the region of the energy gap of the spectrum, where the zero-energy Andreev bound states and their split are seen, generated using* $\Gamma = 0.001$*.*

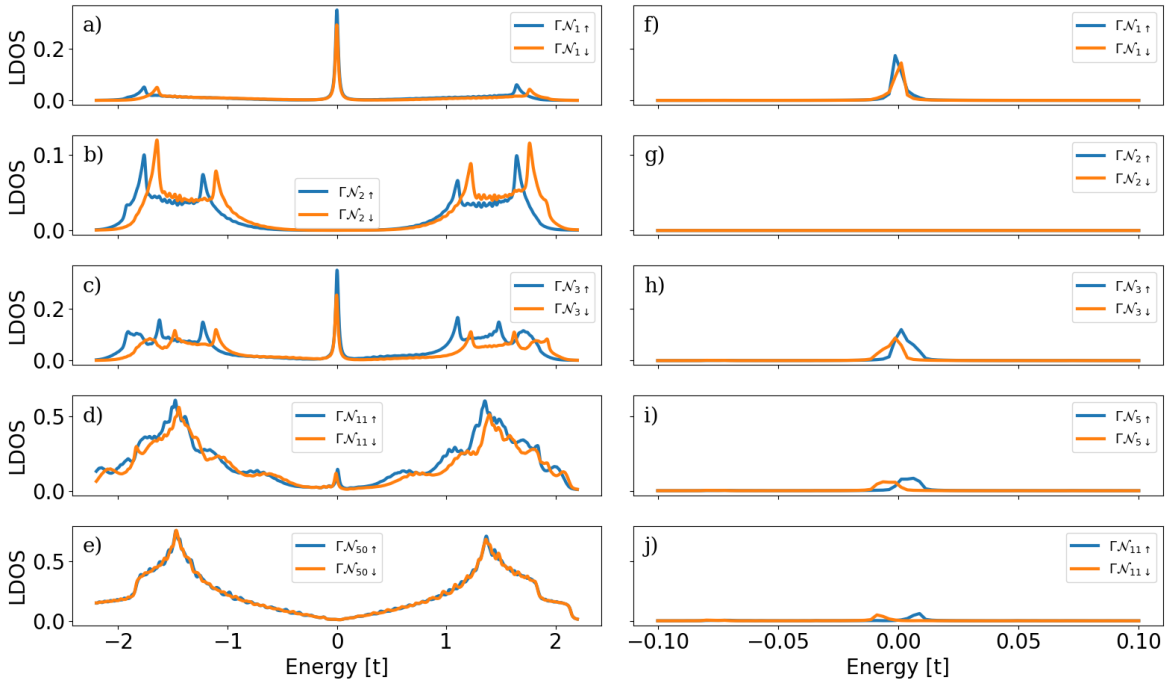

Figure 5.6: *Cuts of the LDOS for sites and spins indicated by the legends. The left colon shows a wider energy spectrum while the right is focused on the gap region. Note that the sites in (d) and (e) are different to (i) and (j). All generated at* $\delta = 0.03$ *and using* $J = 1$.

6 Conclusion and Outstanding Questions

In Chapter 2, the t–J model was introduced and the solution process in a weak-coupling regime outlined in relation to the BCS theory. In Chapter 3, the Gutzwiller approach to the strongly correlated t–J model was presented with special emphasis on the statistically consistent Gutzwiller approach (SGA). A derivation of spin-dependent Gutzwiller factors using counting arguments and fugacity factors was also included in the same chapter. In Chapter 4, the t–J model was analysed in the homogeneous case using the SGA. Phase diagram and density of states (DOS) are presented for the superconducting region and the region with superconductivity coexisting with antiferromagnetism (AFM). In Chapter 5 the SGA was used to solve the t–J model for a slab system with [110] edges. This was done for three different strengths of the exchange-coupling J and different average hole-dopings δ. For all studied cases, the edges were found to attract charge leading to strengthened correlations locally. For the lowest exchange-coupling $J = 0.25$ no s-wave at the edge emerged for $\delta \in [0.05, 0.2]$, but when it was increased to $J = 0.33$ an s-wave started to appear, though much smaller than the s-wave found without charge distribution, see Paper I. By increasing the exchange-coupling further to $J = 1$ and lowering the average hole-doping to $\delta = 0.03$, a solution with coexisting superconductivity and antiferromagnetism at the edge was converged. The average hole doping $\delta = 0.03$ is above the required in bulk for AFM.

The results on superconductivity at the edge raise some further questions about the s-wave. By relaxing the assumption of pure d-wave in the homogeneous case, see Chapter 4, it would be possible to determine if an s-wave is at all present in a bulk system for any J or δ. Together with extended studies on the possible presence of s-wave ordering at higher hole-doping, $J = 0.25$ and $J = 1$, and by determining the doping interval for which the s-wave is present using $J = 0.33$, it could be possible to gain more insights into the influence of the edge on the s-wave.

Further, the importance of the zero-energy Andreev bound states is not concluded. They could in full, partially, or not at all, be responsible for the charging of the edges as they offer low energy states. In that case, the results at [100] edges could be significantly different from those presented in the thesis.

At the studied hole-dopings no AFM is expected in bulk. As charges are drawn to the edges, the occupation in the bulk decreases. It is therefore possible to

imagine, dependent on the size of the system, a situation where the average hole-doping indicates bulk AFM, but the charging of the edges pushes the bulk out of the AFM region.

i

References

[1] H. Bruus and K. Flensberg, *Many-body quantum theory in condensed matter physics - an introduction*, English (Oxford University Press, United Kingdom, 2004) (cit. on pp. 1, 5).

[2] M. Sigrist, "Introduction to unconventional superconductivity", in AIP Conference Proceedings, Vol. 789, 1 (American Institute of Physics, 2005), pp. 165–243 (cit. on pp. 1, 3, 9).

[3] L. N. Cooper, "Bound Electron Pairs in a Degenerate Fermi Gas", Phys. Rev. **104**, 1189–1190 (1956) (cit. on p. 1).

[4] H. K. Onnes, "The resistance of pure mercury at helium temperatures", Commun. Phys. Lab. Univ. Leiden, b **120** (1911) (cit. on p. 1).

[5] B. T. Matthias, T. H. Geballe, and V. B. Compton, "Superconductivity", Rev. Mod. Phys. **35**, 1–22 (1963) (cit. on p. 1).

[6] H. v. Löhneysen, T. Pietrus, G. Portisch, H. G. Schlager, A. Schröder, M. Sieck, and T. Trappmann, "Non-Fermi-liquid behavior in a heavy-fermion alloy at a magnetic instability", Phys. Rev. Lett. **72**, 3262–3265 (1994) (cit. on p. 1).

[7] G. R. Stewart, "Heavy-fermion systems", Rev. Mod. Phys. **56**, 755–787 (1984) (cit. on p. 1).

[8] D. Jérome, A. Mazaud, M. Ribault, and K. Bechgaard, "Superconductivity in a synthetic organic conductor $(TMTSF)_2PF_6$", Journal de Physique Lettres **41**, 95–98 (1980) (cit. on p. 1).

[9] D. D. Osheroff, R. C. Richardson, and D. M. Lee, "Evidence for a New Phase of Solid He^3", Phys. Rev. Lett. **28**, 885–888 (1972) (cit. on p. 2).

[10] D. D. Osheroff, W. J. Gully, R. C. Richardson, and D. M. Lee, "New Magnetic Phenomena in Liquid He^3 below 3 mK", Phys. Rev. Lett. **29**, 920–923 (1972) (cit. on p. 2).

[11] K. M. Seja, "Transport theory and finite element methods for mesoscopic superconducting devices", PhD thesis (Chalmers Tekniska Hogskola (Sweden), 2022) (cit. on p. 2).

[12] J. G. Bednorz and K. A. Müller, "Possible high T c superconductivity in the Ba- La- Cu- O system", Zeitschrift für Physik B Condensed Matter **64**, 189–193 (1986) (cit. on p. 2).

[13] M. K. Wu, J. R. Ashburn, C. J. Torng, P. H. Hor, R. L. Meng, L. Gao, Z. J. Huang, Y. Q. Wang, and C. W. Chu, "Superconductivity at 93 K in a new mixed-phase Y-Ba-Cu-O compound system at ambient pressure", Phys. Rev. Lett. **58**, 908–910 (1987) (cit. on p. 2).

[14] D. J. Van Harlingen, "Phase-sensitive tests of the symmetry of the pairing state in the high-temperature superconductors—Evidence for $d_{x^2-y^2}$ symmetry", Rev. Mod. Phys. **67**, 515–535 (1995) (cit. on p. 3).

[15] C. C. Tsuei and J. R. Kirtley, "Pairing symmetry in cuprate superconductors", Rev. Mod. Phys. **72**, 969–1016 (2000) (cit. on p. 3).

[16] F.-C. Zhang, C. Gros, T. M. Rice, and H. Shiba, "A renormalised Hamiltonian approach to a resonant valence bond wavefunction", Superconductor Science and Technology **1**, 36 (1988) (cit. on pp. 3, 11, 16, 25).

[17] J. Spałek, M. Fidrysiak, M. Zegrodnik, and A. Biborski, "Superconductivity in high-Tc and related strongly correlated systems from variational perspective: Beyond mean field theory", Physics Reports **959**, 1–117 (2022) (cit. on pp. 3, 7).

[18] M. Ogata and A. Himeda, "Superconductivity and antiferromagnetism in an extended Gutzwiller approximation for t–J model: Effect of double-occupancy exclusion", Journal of the Physical Society of Japan **72**, 374–391 (2003) (cit. on pp. 3, 16, 25).

[19] B. Edegger, V. N. Muthukumar, and C. Gros, *Gutzwiller-RVB Theory of High Temperature Superconductivity: Results from Renormalised Mean Field Theory and Variational Monte Carlo Calculations*, 2007, arXiv:0707.1020 [cond-mat.str-el] (cit. on pp. 3, 11, 13).

[20] M. Abram, J. Kaczmarczyk, J. Jędrak, and J. Spałek, "d-wave superconductivity and its coexistence with antiferromagnetism in the t–J–U model: Statistically consistent Gutzwiller approach", Phys. Rev. B **88**, 094502 (2013) (cit. on pp. 3, 16, 17, 19, 25).

[21] J. Jędrak and J. Spałek, "Consistent statistical treatment of the renormalized mean-field $t-J$ model", Phys. Rev. B **81**, 073108 (2010) (cit. on pp. 3, 17, 19).

[22] J. Jędrak and J. Spałek, "Renormalized mean-field t-J model of high-T c superconductivity: Comparison to experiment", Physical Review B **83**, 104512 (2011) (cit. on pp. 3, 17, 19).

[23] H. Tsuchiura, Y. Tanaka, M. Ogata, and S. Kashiwaya, "Local magnetic moments around a nonmagnetic impurity in the two-dimensional $t-J$ model", Phys. Rev. B **64**, 140501 (2001) (cit. on p. 3).

[24] A. Garg, M. Randeria, and N. Trivedi, "Strong correlations make high-temperature superconductors robust against disorder", Nature physics **4**, 762–765 (2008) (cit. on pp. 3, 24).

[25] R. B. Christensen, P. J. Hirschfeld, and B. M. Andersen, "Two routes to magnetic order by disorder in underdoped cuprates", Phys. Rev. B **84**, 184511 (2011) (cit. on pp. 3, 16, 17, 24, 25).

[26] D. Chakraborty and A. Ghosal, "Fate of disorder-induced inhomogeneities in strongly correlated d-wave superconductors", New Journal of Physics **16**, 103018 (2014) (cit. on p. 3).

[27] F. A. Wolf, S. Graser, F. Loder, and T. Kopp, "Supercurrent through Grain Boundaries of Cuprate Superconductors in the Presence of Strong Correlations", Phys. Rev. Lett. **108**, 117002 (2012) (cit. on p. 3).

[28] C. Chen, Y. Chen, Z. D. Wang, and C. S. Ting, "Enhanced superconducting proximity effect in strongly correlated heterostructures", Phys. Rev. B **82**, 174502 (2010) (cit. on p. 3).

[29] H. Tsuchiura, M. Ogata, Y. Tanaka, and S. Kashiwaya, "Electronic states around a vortex core in high-T_c superconductors based on the t-J model", Phys. Rev. B **68**, 012509 (2003) (cit. on p. 3).

[30] Y.-H. Liu, W.-L. Tu, G.-W. Chern, and T.-K. Lee, "Intertwined orders and electronic structure in superconducting vortex halos", Phys. Rev. Res. **5**, 033028 (2023) (cit. on p. 3).

[31] C. Mahato, A. Banerjee, C. Pépin, and A. Ghosal, "Charge modulation in the background of depleted superconductivity inside vortices", Phys. Rev. B **111**, 134519 (2025) (cit. on p. 3).

[32] S. Matsubara and H. Kontani, "Emergence of strongly correlated electronic states driven by the Andreev bound state in d-wave superconductors", Phys. Rev. B **101**, 075114 (2020) (cit. on p. 3).

[33] S. Matsubara and H. Kontani, "Emergence of $d \pm ip$-wave superconducting state at the edge of d-wave superconductors mediated by ferromagnetic fluctuations driven by Andreev bound states", Phys. Rev. B **101**, 235103 (2020) (cit. on p. 3).

[34] D. Chakraborty, T. Löfwander, M. Fogelström, and A. M. Black-Schaffer, "Disorder-robust phase crystal in high-temperature superconductors stabilized by strong correlations", npj Quantum Materials **7**, 44 (2022) (cit. on pp. 3, 16, 17, 38).

[35] Y. Chen, M. D. Croitoru, A. A. Shanenko, and F. M. Peeters, "Superconducting nanowires: quantum confinement and spatially dependent Hartreeâ€"Fock potential", Journal of Physics: Condensed Matter **21**, 435701 (2009) (cit. on p. 3).

[36] Y. Tanuma, Y. Tanaka, M. Ogata, and S. Kashiwaya, "Quasiparticle states near surfaces of high$-T_c$ superconductors based on the extended $t - J$ model", Phys. Rev. B **60**, 9817–9826 (1999) (cit. on pp. 3, 37).

[37] J.-X. Zhu, *Bogoliubov-de Gennes method and its applications*, Vol. 924 (Springer, 2016) (cit. on pp. 6, 22, 24).

[38] K. Chao, J Spałek, and A. Oles, "Kinetic exchange interaction in a narrow S-band", Journal of Physics C: Solid State Physics **10**, L271 (1977) (cit. on p. 7).

[39] P. Fazekas, *Lecture notes on electron correlation and magnetism*, Vol. 5 (World scientific, 1999) (cit. on p. 7).

[40] M. C. Gutzwiller, "Effect of Correlation on the Ferromagnetism of Transition Metals", Phys. Rev. Lett. **10**, 159–162 (1963) (cit. on p. 11).

[41] N. Lanatà, H. U. R. Strand, X. Dai, and B. Hellsing, "Efficient implementation of the Gutzwiller variational method", Phys. Rev. B **85**, 035133 (2012) (cit. on p. 11).

[42] N. Fukushima, "Grand canonical Gutzwiller approximation for magnetic inhomogeneous systems", Phys. Rev. B **78**, 115105 (2008) (cit. on pp. 11, 12, 16).

[43] M. Abram, M. Zegrodnik, and J. Spałek, "Antiferromagnetism, charge density wave, and d-wave superconductivity in the extended t-J-U model: role of intersite Coulomb interaction and a critical overview of renormalized mean field theory", Journal of Physics: Condensed Matter **29**, 365602 (2017) (cit. on pp. 12, 19, 25).

[44] W.-H. Ko, C. P. Nave, and P. A. Lee, "Extended Gutzwiller approximation for inhomogeneous systems", Physical Review B **76**, 245113 (2007) (cit. on p. 16).

[45] D. Chakraborty, "Disorder-induced Inhomogeneities in Strongly Correlated d-wave Superconductors", PhD thesis (Indian Institute of Science Education and Research Kolkata, 2017) (cit. on p. 16).

[46] W.-L. Tu, "Renormalized Mean Field Theory", in *Utilization of Renormalized Mean-Field Theory upon Novel Quantum Materials* (Springer, Singapore, 2019), pp. 21–31 (cit. on p. 17).

[47] J. Kaczmarczyk and J. Spałek, "Coexistence of antiferromagnetism and superconductivity within t-J model with strong correlations and nonzero spin polarization", Phys. Rev. B **84**, 125140 (2011) (cit. on p. 17).

[48] J. Kaczmarczyk, "Comparison of two approaches for the treatment of Gutzwiller variational wave functions", Philosophical Magazine **95**, 563–573 (2015), eprint: `https://doi.org/10.1080/14786435.2014.965235` (cit. on p. 17).

[49] L. E. Reichl, *A modern course in statistical physics* (Wiley, 1998) (cit. on p. 22).

[50] X. Zhou, W.-S. Lee, M. Imada, N. Trivedi, P. Phillips, H.-Y. Kee, P. Törmä, and M. Eremets, "High-temperature superconductivity", Nature Reviews Physics **3**, 462–465 (2021) (cit. on p. 25).